HHS Public Access

Author manuscript

Cell Rep. Author manuscript; available in PMC 2024 March 26.

Published in final edited form as:

Cell Rep. 2024 February 27; 43(2): 113670. doi:10.1016/j.celrep.2023.113670.

The integrated stress response effector GADD34 is repurposed by neurons to promote stimulus-induced translation

Mauricio M. Oliveira[1], **Muhaned Mohamed**[1], **Megan K. Elder**[1], **Keylin Banegas-Morales**[1], **Maggie Mamcarz**[1], **Emily H. Lu**[1], **Ela A.N. Golhan**[1], **Nishika Navrange**[1], **Snehajyoti Chatterjee**[2], **Ted Abel**[2], **Eric Klann**[1,3,4,*]

[1]Center for Neural Science, New York University, New York, NY, USA

[2]Department of Neuroscience and Pharmacology, Carver College of Medicine, University of Iowa, Iowa City, IA 52242, USA

[3]NYU Neuroscience Institute, New York University School of Medicine, New York, NY, USA

[4]Lead contact

SUMMARY

Neuronal protein synthesis is required for long-lasting plasticity and long-term memory consolidation. Dephosphorylation of eukaryotic initiation factor 2α is one of the key translational control events that is required to increase *de novo* protein synthesis that underlies long-lasting plasticity and memory consolidation. Here, we interrogate the molecular pathways of translational control that are triggered by neuronal stimulation with brain-derived neurotrophic factor (BDNF), which results in eukaryotic initiation factor 2α (eIF2α) dephosphorylation and increases in *de novo* protein synthesis. Primary rodent neurons exposed to BDNF display elevated translation of GADD34, which facilitates eIF2α dephosphorylation and subsequent *de novo* protein synthesis. Furthermore, GADD34 requires G-actin generated by cofilin to dephosphorylate eIF2α and enhance protein synthesis. Finally, GADD34 is required for BDNF-induced translation of synaptic plasticity-related proteins. Overall, we provide evidence that neurons repurpose GADD34, an effector of the integrated stress response, as an orchestrator of rapid increases in eIF2-dependent translation in response to plasticity-inducing stimuli.

Graphical Abstract

*Correspondence: ek65@nyu.edu.

AUTHOR CONTRIBUTIONS

M.M.O. and E.K. conceptualized and designed the project. M.M.O., M.K.E., M. Mohamed, K.B.-M., M. Mamcarz, E.H.L., E.A.N.G., N.N., and S.C. designed, performed, and analyzed experiments. M.M.O. and E.K. wrote and edited the manuscript. T.A. and E.K. contributed animals, materials, and analysis tools.

DECLARATION OF INTERESTS

The authors declare no competing interests.

SUPPLEMENTAL INFORMATION

Supplemental information can be found online at https://doi.org/10.1016/j.celrep.2023.113670.

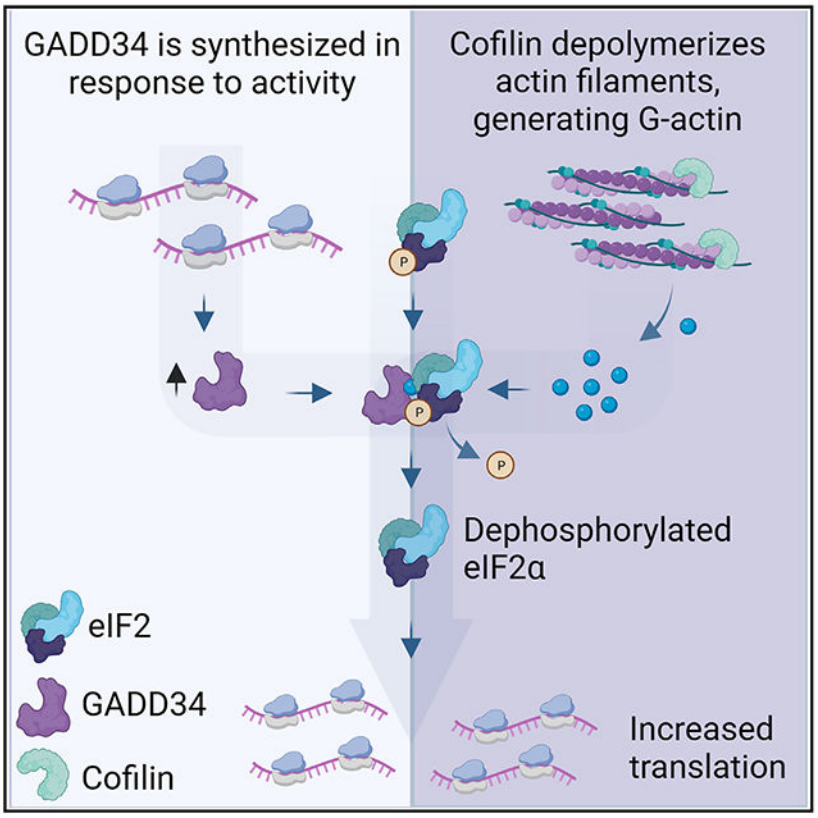

In brief

Oliveira et al. demonstrate that sharp increases in protein synthesis resulting from neuronal activation require GADD34-induced eIF2α dephosphorylation. GADD34 expression is tied to the regulation of mRNA translation. Neuronal GADD34 then recruits actin monomers to stabilize its interaction with eIF2α and promote its dephosphorylation.

INTRODUCTION

In 1964, Flexner and colleagues[1] demonstrated that long-term memory formation relies on the synthesis of new proteins. Since then, increasing evidence has demonstrated that rapid increases in neuronal *de novo* protein synthesis are critical for memory consolidation.[2] Moreover, dysregulation of protein synthesis is a central feature in several neurodevelopmental and neurode-generative disorders.[3-13] These observations have generated intense interest regarding how neurons control translation in response to activity and how this contributes to brain function, including cognitive function.

Cis-regulatory elements present at untranslated regions (UTRs) flanking the main open reading frame (ORF) localize mRNAs throughout subcellular compartments, conferring the evolutionary advantage of rapid proteome modifications locally without the need for protein trafficking.[14-20] In neurons, this becomes even more pronounced due to their extensive projections; 90% neuronal proteome is located at these projections.[21] In recent years, great effort has been directed toward identifying the mRNAs that are translated in dendrites and

axons, which has revealed mRNAs that encode structural-plasticity-related proteins located to synapses, such as cytoskeleton modifiers, post-synaptic density scaffolding components, and ribosomal proteins.[22-28] Overall, these findings suggest that *de novo* protein synthesis coordinates a number of processes involved in synaptic development and transmission, such as ion channel insertion/depletion in the post-synaptic density,[29-32] dendritic spine expansion,[33-36] pre-synaptic arbor development,[37-39] axon growth,[39-43] and neurotransmitter release.[44-46]

The translation of both somatic and dendritic mRNAs is enhanced in response to extracellular stimuli, including neurotransmitters and neurotrophins. These include brain-derived neurotrophic factor (BDNF), which is released in a calcium-dependent manner,[47,48] binding to post-synaptic tyrosine kinase receptors and triggering at least two major pathways that can promote protein synthesis: extracellular-regulated kinase (ERK) and mechanistic target of rapamycin complex 1 (mTORC1)-mediated pathways,[49-52] which promote translation of mRNAs via eukaryotic initiation factor 4E (eIF4E) and eEF2.[51,53-55] BDNF also can induce protein-synthesis-dependent long-term potentiation in the hippocampus,[49,56-61] dendritic spine expansion,[35,62] and calcium-dependent release of neurotransmitters.[44,60] Thus, release of BDNF can trigger synaptic signaling to increase *de novo* protein synthesis.

Despite the identification of mRNAs localized to dendrites, how these quiescent mRNAs become translated in response to plasticity-inducing stimuli is still an open question. Translation is a multi-step and -factorial process with an overwhelming number of regulatory checkpoints. Neuronal translation initiation is regulated at two main checkpoints: the phosphorylation of the eIF2 on its alpha subunit (eIF2α-P) and the phosphorylation of eIF4E/4E-binding protein 2 (4E-BP2).[63] eIF4E has been implicated in plasticity-related events, stimulating the translocation of ribosomes from the dendritic shaft to spines[64] and promoting synthesis of proteins that are known to be important for synaptic and memory consolidation.[65] eIF4E mRNA and protein also were shown to be enriched in dendritic spines during memory formation.[66,67]

The first step of translation initiation requires eIF2, which is responsible for carrying loaded ^{Met}tRNA-Met to ribosomes. The transfer of the amino acid from tRNA to the nascent peptide chain requires guanosine triphosphate (GTP) to be bound by eIF2, which is promoted by the guanosine exchange factor eIF2B.[68-72] When phosphorylated on its α subunit (eIF2α-P), eIF2 blocks the exchange activity of eIF2B and inhibits global translation.[73] The phosphorylation of eIF2α is critical for the integrated stress response (ISR), which is triggered by different cellular stressors. These stressors converge to rapidly increase eIF2α-P levels via activation of protein kinases that sense stress, resulting in an inhibition of general protein synthesis to conserve energy until the cellular stress is resolved. The reduction of protein synthesis coincides with the translation of a subset of mRNAs with upstream ORFs (uORFs) in their 5′ UTR.[74] One such mRNA, *Ppp1r15a,* encodes GADD34, a scaffolding protein that acts in a negative feedback loop to the ISR. GADD34 is a protein phosphatase 1 (PP1)-targeting protein that directly binds to eIF2α-P, thereby promoting its dephosphorylation and restoration of protein synthesis after stress resolution.[75]

Decreased levels of eIF2α-P are associated with neuronal activity and memory formation. Long-term potentiation (LTP)[76] and threat conditioning in the basolateral amygdala[77] and hippocampus[78] are associated with decreased levels of eIF2α-P. Moreover, it was shown that blocking the decrease in eIF2α-P following learning impairs long-term memory consolidation.[79] At the cellular level, eIF2α phosphorylation controls spine expansion[80] and promotes the insertion of AMPAR in the post-synaptic density.[29] However, the mechanism responsible for the plasticity-induced downregulation of eIF2α-P remains unknown. We considered two main hypotheses: plasticity-inducing stimulation (1) decreases eIF2α kinase activity, resulting in reduced eIF2α-P, and/or (2) increases eIF2α dephosphorylation via alteration of regulators of the phosphatase. Because the latter offers a direct and more rapid way of altering eIF2α-P (instead of kinase inhibition followed by passive dephosphorylation), we hypothesized that neuronal activation results in GADD34-mediated dephosphorylation of eIF2α, thereby increasing protein synthesis after neuronal activity. Herein, we provide evidence that neuronal stimulation with BDNF increases GADD34 expression in neurons and that this increase relies on translational, rather than transcriptional, regulation. Moreover, BDNF increases the physical interaction between GADD34 and eIF2α in both soma and dendrites, and GADD34 expression converges with actin cytoskeleton dynamics, which is required for the BDNF-induced increase in protein synthesis. Finally, GADD34 orchestrates the translation of numerous mRNAs related to neurotransmission-related metabolic functions as well as synaptic organization and activity. Overall, our findings support the notion that activity-dependent increases in neuronal protein synthesis rely on translation-dependent increases in GADD34 expression, revealing a molecular mechanism by which neuronal activation promotes rapid *de novo* translation.

RESULTS

GADD34 is constitutively expressed in neurons

GADD34 has classically been described as a negative regulator of the ISR, expressed solely under stress conditions, but a cell-type-specific RNA sequencing (RNA-seq) database showed that GADD34 mRNA is present in neurons, microglia, and astrocytes in the mouse brain.[75,81] These findings prompted us to determine whether GADD34 is constitutively expressed in neurons.

We first employed fluorescence *in situ* hybridization (FISH) RNA scope to verify presence and localization of *Ppp1r15a* mRNA (which encodes GADD34) in primary neurons. We found that *Ppp1r15a* mRNA is localized in both the soma (~75% total FISH signal) and dendrites (~25%) of mature (days *in vitro* [DIV] 14) mouse cortical neurons (Figures 1A and 1B). Treatment with the stressor thapsigargin showed that the signal was specific to *Ppp1r15a* mRNA (Figures S1A-S1D). To study protein expression in the cell reliably (i.e., confirmation of specific antibody staining), we targeted GADD34 expression in a cell-type-specific way, engineering a new viral tool that allowed the expression of a short hairpin RNA (shRNA) targeting *Ppp1r15a* mRNA in a Cre-dependent manner using the AAV9. EF1.mCherry.SICO-shRNA.*Ppp1r15a* (Figure 1C). With this virus, we selectively decreased the expression of GADD34 in excitatory neurons, employing a viral cocktail composed of AAV9.CamKIIα-Cre driver and AAV9.EF1.mCherry.SICO-shRNA.*Ppp1r15a*,

when compared to neurons transduced with the control AAV9.hSyn.DIO.mCherry (DIO = double-floxed inverted ORF; Figure 1D). Using this approach, we were able to transduce 31% of neurons with the shRNA (Figure S1E), from which 78.6% express the shRNA (Figure S1F). We then evaluated whether GADD34 protein could be detected in neurons with immunocytochemistry. We found that GADD34 is expressed in both soma and dendrites of neurons and that this expression was downregulated when neurons expressed the shRNA targeting GADD34 (Figures 1E and 1F). We further confirmed these results with western blot analysis of neurons transduced with the viral cocktail and found that GADD34 protein expression was significantly reduced by the shRNA (Figure 1G). Surprisingly, we did not observe significant alterations in eIF2α-P levels, suggesting that GADD34 plays a minimal role in basal neuronal translation initiation (Figure 1H). Overall, these results confirmed that GADD34 is constitutively expressed in neurons.

BDNF increases GADD34 translation in neurons

GADD34 was previously shown to have its expression in neurons tied to plasticity-related transcription factors.[82,83] Therefore, we hypothesized that neuronal stimulation could increase GADD34 levels in primary neurons. To address this question, we induced translation-dependent activity in primary neurons using BDNF.[56] We exposed primary neurons to BDNF (50 ng/mL) for 0, 5, 15, 30, 60, or 120 min and then probed for GADD34 protein levels via western blot. We found that GADD34 was significantly increased 60 min after exposure to BDNF and that this increase, which was accompanied by a concomitant decrease in eIF2α-P levels (Figures 2A-2C), persisted until at least 120 min, suggesting that GADD34 could be a direct mediator of BDNF-induced decreases in eIF2α-P. These findings indicated that neuronal GADD34 expression can be induced by BDNF.

Our results and previous data[84] showed that GADD34 mRNA (*Ppp1r15a*) is present both in soma and dendrites of neurons (Figure 1). We then examined whether the increase in GADD34 levels was compartmentalized. We first determined total levels of GADD34 in somatic vs. dendritic compartments of neurons treated with BDNF (Figure 2D) and performed a radial quantification of GADD34 staining in dendritic arbors (Figure 2E). Our results indicated that GADD34 protein levels are increased in dendrites, but not the soma, 1 h after stimulation with BDNF (Figures 2F and 2G). We then asked whether the increase in GADD34 expression was due to transcriptional modulation, as BDNF is suggested to increase ATF4 in neurons.[85] We observed no differences between *Ppp1r15a* mRNA levels after exposure to BDNF (Figures 2H-2K). Moreover, when we pre-treated neurons with cycloheximide (Figure 2L), a potent translation inhibitor, BDNF failed to increase GADD34 levels (Figure 2M) or to decrease eIF2α-P (Figure 2N). Thus, these data suggest that the increase in BDNF-induced increase in GADD34 levels relies on translation.

Previous ribosome footprinting data indicate that *Ppp1r15a* mRNA is loaded into neuronal ribosomes in both somatic and dendritic compartments but is preferentially stalled at the uORFs in the 5′ UTR of the mRNA (Figure 3A).[84] We combined this observation with our data (Figure 2M) and hypothesized that GADD34 protein levels are increased by BDNF via regulation at the translational level. To test this hypothesis, we performed translating ribosome affinity purification (TRAP) to investigate changes in the amount

of *Ppp1r15a* mRNA loaded onto ribosomes of excitatory neurons exposed to BDNF (Figure 3B; see STAR Methods).[86] We transduced primary neurons with a viral cocktail containing AAV9.CamKIIα-Cre and AAV9.CAG.FLEX. L10a-EGFP to drive L10a-EGFP expression in excitatory neurons, which resulted in transduction of ~75% neurons (Figures S2A-S2C). Real-time PCR demonstrated that the amount of *Ppp1r15a* bound to ribosomes was significantly increased in response to BDNF (Figure 3C, brown points). Curiously, when we examined total *Ppp1r15a* mRNA, we found a (non-significant) trend for enhanced levels following BDNF, also suggesting a transcriptional event in response to BDNF (Figure 3C, blue points). However, it should be noted that this increase could also arise from either inhibitory neurons or glial cells that are present in the primary cultures we utilized.

To gain deeper knowledge on *Ppp1r15a* translation regulation, we performed a polysome fractionation with sucrose gradients; collected fractions representing monosomes, disomes, trisomes, or heavy polysomes (4 or more); and measured total *Ppp1r15a* mRNA per fraction. Our data indicated that the occupancy of *Ppp1r15a* in the heavier fractions was higher when cells were exposed to BDNF, suggesting higher translation rates (Figures 3D-3F). Finally, we used proximity ligand assay (PLA) coupled to puromycilation (puro-PLA)[87] to visualize amounts and localization of newly synthesized GADD34 in neurons (Figures 3G and S2D-S2F). To determine whether *Ppp1r15a* mRNA is translated during BDNF stimulation, we treated neurons for 0, 5, 30, 60, and 120 min with BDNF, and added puromycin during the last 5 min, to obtain a snapshot of GADD34 translation (Figure 3G; refer to STAR Methods for details regarding the quantification process). Strikingly, the synthesis of GADD34 peaked 60 min after exposure to BDNF (Figure 3H). Furthermore, compartment-specific analysis showed elevated GADD34 translation after exposure to BDNF in both soma and dendrites (Figures 3I-3K). Altogether, these results demonstrate that the increase in GADD34 levels induced by BDNF are due to translational, rather than transcriptional, regulation.

BDNF promotes GADD34-eIF2α interactions and GADD34-dependent protein synthesis

Previous work demonstrated that neuronal activity increases protein synthesis via reduced eIF2α-P.[76,77] Therefore, we asked whether GADD34 was required for the BDNF-induced decrease in eIF2α-P and increase in protein synthesis. We first determined whether BDNF could promote interactions between GADD34 and eIF2α. To assess this, we used PLA, this time targeting GADD34 and eIF2α. We found that the PLA was a reliable approach to measure GADD34-eIF2α interactions, as thapsigargin significantly increased the PLA signal (Figures S3A and S3B). To obtain a spatiotemporal analysis of GADD34-eIF2α interactions, we exposed neurons to BDNF for 0, 5, 15, 30, and 60 min prior to fixation and subsequent PLA analysis (Figures S3C-S3E). We found that the GADD34-eIF2α interactions peak at 60 min (Figure S3E, black dashed line). Notably, we observed that the PLA signal peaked at 30 min in the dendritic compartment (Figure S3E, red dashed line), whereas in the soma, the peak was at later time points (Figure S3E, blue dashed line) after BDNF stimulation. Compartment-specific analysis of the PLA signal induced by BDNF revealed that the GADD34-eIF2α interaction was increased after 60 min BDNF stimulation in both soma and dendrites (Figures 4A and 4B). These findings indicate that BDNF increases GADD34-eIF2α interactions.

To determine whether GADD34 is also required for BDNF-dependent increases in neuronal protein synthesis, we transduced neurons with a viral cocktail containing AAV9.CamKIIα-Cre and either AAV9.EF1.mCherry.SICO-shRNA.*Ppp1r15a* or AAV9. hSyn.DIO.mCherry (control). We then tested whether GADD34 mediated the BDNF-dependent decrease in eIF2α-P. We found that decreasing GADD34 expression blocked eIF2α dephosphorylation (Figures 4F, 4G, S3F, and S3G) as well as the increase in protein synthesis by BDNF (Figures 4H and 4I) as assessed by surface sensing of translation (SUnSET; Figure S3H).[88] Notably, and consistent with results described in Figure 1, we found no baseline differences in either eIF2α-P or *de novo* protein synthesis due to ablation of GADD34 (Figures 4G and 4I, light green bars). Collectively, our data indicate that GADD34 is necessary for the BDNF-induced increase in protein synthesis via eIF2α dephosphorylation.

GADD34 mediates the BDNF-induced translation of synaptic-plasticity-related mRNAs

Thus far, our data suggest that GADD34 is required for BDNF-induced protein synthesis. Therefore, we proceeded to determine the identity of the mRNAs whose translation is regulated in a GADD34-dependent manner with TRAP-seq, which allowed us to identify mRNAs specifically in excitatory neurons. We transduced neurons harboring *flox* inserts in the first two exons of GADD34 with AAV9.CamKIIα.Cre (henceforth called “KO” [knockout] cells) and AAV9.CamKIIα.EGFP-L10a. As a control for the Cre recombinase (henceforth termed “WT” [wild-type] cells), we used AAV9.CamKIIα.mCherry (Figure S4A). At DIV 14, these neurons were exposed to BDNF for 1 h, samples were collected, and ribosomes were purified using GFP antibodies (see STAR Methods). Using this method, we found that 784 mRNAs were differentially expressed (DEGs [differentially expressed genes]) in the total lysate of WT cells (425 upregulated and 359 downregulated by BDNF) (Figure 5A), whereas 3,815 were DEGs in the TRAP-purified samples (1,878 upregulated and 1,937 downregulated by BDNF) (Figure 5B; for full list of DEGs, see Table S1). Furthermore, we found no significant outliers among samples using both principal-component analysis (PCA; Figure S4B) and unsupervised clustering (Figure S4C). When we measured the correlation between total mRNA $\log_2$ fold change ($\log_2$FC) vs. TRAP $\log_2$FC, we found a small correlation (Pearson’s correlation coefficient = 0.1481) (Figure 5C), indicating that changes in the pool of mRNAs being differentially translated after 1 h BDNF exposure were not explained by transcriptional changes. Of note, the analysis of DEGs obtained showed an enrichment for markers of excitatory neurons (*Camk2a, Grin1, Slc17a5,* and *Slc17a7*) in the purified samples over total lysate, as well as a depletion of markers of inhibitory neurons (*Pvalb, Gad1*) and glial cells (*Gfap, Cnp*) (Figure S4D).

We then determined the expression of immediate-early genes (IEGs) induced by BDNF in WT cells and found robust increases in all IEGs investigated in both TRAP and total mRNA fractions, showing expected plasticity-related transcriptional activation (Figure 5D). Gene Ontology (GO) analysis of the DEGs upregulated by BDNF revealed an enrichment of GOs related to neuronal development, synaptic organization, and signaling cascades, including MAPK, which is known to be activated by BDNF (Figure 5E; Table S2). We then asked whether this enrichment was specific to ribosomal fraction or whether it represented a transcriptional change (i.e., overrepresentation in the total mRNA). We isolated the identity of mRNAs from two enriched GOs (“synapse organization” and “positive regulation

of MAPK cascade") and compared their log_2FC with the log_2FC from the mRNAs identified in the sequencing (Figures S4E and S4F). This comparison demonstrated that the enrichment is specific to the purified fraction, with no prominent changes found in the total mRNA (Figures 5F and 5G). The GO analysis of mRNAs that were downregulated, on the other hand, revealed an enrichment of GOs related mostly to metabolic activities, such as "ribosome" or "mitochondrion organization" (Figure 5H; Table S2). When we compared the components from the GOs "ribosome" against the change of all mRNAs, we found a ribosomal-fraction-specific depletion of ribosomal protein transcripts (Figure 5I). Surprisingly, they were enriched in the total fraction when compared against all mRNAs (Figures 5J and S4G). Comparison of the GO "microtubule" components did not show any significant enrichment in either fraction (Figures 5J and S4H).

To determine the identity of mRNAs that directly rely on GADD34 to be translated, we plotted the log_2FCs of all mRNAs shared in the sequencing of WT over KO cells (Figure 5K). Again, overall distribution showed no obvious correlation between samples, but it allowed us to identify mRNAs that were upregulated (blue dots) or downregulated (orange dots) in WT cells exposed to BDNF but that were not significantly changed in KO cells treated the same way ("corrected" mRNAs). GO analysis of the "corrected" mRNAs that were upregulated in the WT cells indicated that they were mostly related to either synaptic composition or synapse activity (Figure 5L). The downregulated "corrected" mRNAs, on the other hand, were mostly related to mitochondrial activity or ribosomes (Figure 5M). Comparing the FCs of the candidate GOs "synaptic organization" and "positive regulation of MAPK cascade" revealed that transcripts were enriched in the total fraction of KO cells vs. WT, whereas the opposite was true for the purified fraction (Figure 5N). On the other hand, comparison of the mRNAs that belong to the GO "ribosome" showed an enrichment in the total fraction of WT when compared to KO, and this relationship was inverted in the purified fraction. (Figure 5O). Again, the GO "microtubule" showed no detectable difference between FCs of WT and KO (Figure 5O). Overall, these results reveal a central role for GADD34 in the BDNF-induced synthesis of proteins that are directly involved in synaptic plasticity and highlight that eIF2-dependent translation initiation is a key pathway that mediates BDNF-dependent synaptic plasticity.

Notably, BDNF stimulation significantly affects the translatome in GADD34 KO cells, as we found 2,662 DEGs in the TRAP fraction (1,162 upregulated, 1,500 downregulated) and 411 in the total mRNA fraction (225 upregulated, 186 downregulated) (Figures S4I and S4J; Table S1). Indeed, when we isolated IEG FCs, we found no obvious alteration in the induction of IEGs when compared to controls (Figure S4K; total mRNA fraction not shown). However, bioinformatic analysis revealed no outstanding GO being altered among upregulated mRNAs in the TRAP fraction. On the other hand, mRNAs related to the GO "post-synapse" were downregulated after stimulation with BDNF. We then compared the FCs between WT and KO cells of genes with the GOs "synaptic organization" (upregulated in WT) and "post-synapse" (downregulated in KO) and found that the upregulation seen in the TRAP fraction was not present in the total mRNA fraction (Figure 5P), suggesting dysfunction at the translational level. In summary, these results suggest that BNDF-induced plasticity relies on a translational program driven by the GADD34-eIF2α axis.

BDNF increases interactions between G-actin and GADD34

The fact that GADD34 can rapidly promote eIF2α dephosphorylation following neuronal stimulation with BDNF indicates that this process could be integrated with early events involved in synaptic consolidation. Notably, to effectively bind to eIF2α, GADD34 must interact with G-actin, which stabilizes the GADD34-eIF2α interaction.[89,90] Indeed, a SynGO analysis of mRNAs significantly changed in the TRAP-seq showed that the subgroup "actin cytoskeleton dynamics" is overrepresented (Figure S5A, highlighted quadrants). An in-depth analysis of the mRNAs showed no specific enrichment in the sequencing (Figure S5B). The change in *Cfl1,* however, caught our attention due to its central role in reshaping the actin cytoskeleton during early synaptic plasticity.[91] We hypothesized that BDNF could promote actin destabilization through cofilin, leading to increased interactions between GADD34 and G-actin. Consistent with this idea, stimulation of neurons with BDNF for 1 h resulted in a significant decrease in phosphorylated cofilin (Figures 6A-6C). Surprisingly, though, this decrease is not due to changes in phosphorylation per se (Figure 6C) but is rather due to increased amounts of total cofilin (Figure 6D).

Because cofilin promotes the conversion of F-actin into G-actin, we asked whether BDNF could increase GADD34-actin interactions. A PLA showed that BDNF increased the interaction between both proteins (Figures 6E and 6F). To verify that the observed interaction was due to G- rather than F-actin, we used latrunculin A to sequester G-actin, rendering it unavailable for protein interactions.[92-94] The sequestration of G-actin completely ablated the GADD34-actin PLA signal (Figures S5C and S5D). Finally, knockdown of cofilin with targeted shRNA (Figures S5E and S5F) blocked the increase in GADD34-eIF2α interactions induced by BDNF (Figures 6G and 6H) without modifying the total protein levels of GADD34 (Figures S5G and S5H). Overall, these results demonstrate that BDNF increases cofilin activity, facilitating physical interaction between eIF2α and GADD34.

Increasing cofilin activity promotes eIF2α dephosphorylation and protein synthesis

Because BDNF decreased the ratio between phosphorylated cofilin and total cofilin (Figures 6A-6D) and promoted GADD34-G-actin interactions (Figures 6E and 6F) that mediate binding of GADD34 to eIF2α, we examined whether cofilin activity could act as a modulator of eIF2-dependent translation. To determine whether increased cofilin activity is sufficient to increase GADD34-eIF2α interactions, we transduced primary neurons with two viral vectors bearing overexpressing systems, AAV5. CamKIIα.cofilin-WT-HA (cof-WT) or AAV5.CamKIIα.cofilin-S3A-HA (cof-S3A) (Figure 7A), where the former increases the amount of total cofilin inside the cell and the latter results in the overexpression of a hyperactive, phospho-dead mutant cofilin[95] (Figures S6A-S6E). Using this system, we verified that the G-/F-actin ratio was increased when cof-S3A was overexpressed (Figures S6F and S6G).

We then determined whether the overexpression of either cof-WT or cof-S3A changed total levels of GADD34 and eIF2ya-P. Expression of either type of cofilin did not alter expression of GADD34 (Figure 7B), whereas both caused downregulation of eIF2α-P (Figure 7C).

These findings suggest that cofilin promotes increased GADD34-eIF2α interactions through an increase in available G-actin. We thus performed a PLA for GADD34-eIF2α in neurons transduced with either cof-WT or cof-S3A and found that overexpression of both forms of cofilin enhanced GADD34-eIF2α interactions (Figures 7D and 7E). Our results led us to test whether cofilin overexpression could increase basal translation. Our results indicated that cof-S3A, but not cof-WT, significantly increased neuronal translation (Figures 7F and 7G, light-colored points). However, when stimulated with BDNF, neurons transduced with cof-WT showed increased translation when compared to non-transduced neurons stimulated the same way (Figures 7F and 7G, dark-colored points). Finally, we queried whether the cofilin-dependent increase in protein synthesis is mediated by GADD34. To investigate this, we obtained primary neurons from GADD34$^{fl/fl}$ mice and transduced them with two viruses: (1) CamKIIyα.Cre, to ablate the expression of GADD34 in excitatory neurons, and (2) no virus, cof-WT, or cof-S3A. Strikingly, we found that the ablation of GADD34 blocked the increase in *de novo* protein synthesis mediated by cof-S3A (Figures 7H and 7I). Altogether, these data demonstrate that increasing the amount of available G-actin triggers a GADD34-dependent increase in protein synthesis.

DISCUSSION

Here, we interrogated the molecular mechanisms that contribute to rapid changes in neuronal *de novo* translation due to activity. Among the conserved checkpoints for translation is the dephosphorylation of eIF2α, which is critical for many forms of long-lasting synaptic plasticity and memory consolidation.[2] Rapid dephosphorylation of eIF2α occurs in CamKIIα-expressing excitatory neurons and somatostatin-expressing interneurons in the hippocampus following contextual threat conditioning[78] and in CamKIIα-expressing principal neurons in the lateral amygdala.[77,79] Accordingly, chemogenetic-induced transient increases in eIF2α-P during early stages of memory consolidation can impair that process.[79] Our results indicate that translation of GADD34 and cytoskeleton dynamics converge to promote activity-dependent eIF2α dephosphorylation within an hour, thereby driving increases in neuronal translation, including the synthesis of proteins closely related to synaptic remodeling and consolidation.

Plasticity-related dephosphorylation of eIF2α relies on GADD34 activity

Despite demonstration that dephosphorylation of eIF2α contributes to long-lasting plasticity and long-term memory formation, a molecular mechanism for eIF2α dephosphorylation in these contexts had not been identified. Herein, we provide evidence that GADD34, a scaffolding protein that mediates eIF2α dephosphorylation by PP1,[96] is responsible for rapid BDNF-induced dephosphorylation of eIF2α. Our findings offer an attractive explanation as to how BDNF shapes the neuronal proteome shortly after activation. We show that BDNF increases the levels of GADD34 and decreases eIF2α-P levels in primary neurons. Furthermore, BDNF promotes the physical interaction of GADD34 with eIF2α, (Figure 4), which is required for decreased levels of eIF2α-P. We cannot exclude the possibility that simultaneous events are occurring upstream to silence the eIF2α kinases given that PKR, GCN2, and PERK (all eIF2α kinases) have been shown to mediate learning and memory.[97-102] We propose that GADD34 rapidly promotes eIF2α dephosphorylation in

neurons but that the downregulation of eIF2α96 kinases represents a long-term solution to keep translation at a higher rate during late phases of consolidation. This is supported by the notion that GADD34 has a high turnover rate due to the Δpest domains in its structure,[96] although these are thought to modulate PP1 activity rather than promote GADD34 degradation.[103] Moreover, we also cannot rule out an orchestrated mechanism involving GADD34 and its counterpart, the constitutive repressor of eIF2α-P (CReP), to drive translation upregulation during memory consolidation, as both proteins were shown to have complementary effects in the unfolded protein response,[104] and CReP has been demonstrated to have a role in synaptic plasticity and long-term memory formation.[105] Further studies are necessary to determine whether neuronal eIF2α dephosphorylation following activity is, in fact, a multi-factorial process and whether it is a long-lasting or acute episode triggered by neuronal activation.

Understanding the molecular pathways that underlie activity-dependent translation initiation and their subcellular localization is key to unraveling the initial steps of neuronal response to synaptic stimulation. Proteomic studies suggest that BDNF increases the amount of translation initiation factors in dendritic compartments.[106] In addition, previous studies showed that a rapid, but transient, MNK1-mediated phosphorylation of eIF4E occurs when synaptodendrosomes were exposed to BDNF, which was correlated with an upregulation of *de novo* translation.[49,65] Remarkably, our TRAP-seq revealed that effectors and targets of the ERK and mTORC1 pathways seem to be consistently modulated by BDNF through GADD34, as demonstrated by the changes in translating mRNAs related to translation and MAPK signaling, indicating a cross-regulation between these translation-promoting pathways. Notably, there is no evidence suggesting that eIF2 subunits are enriched in dendrites after potentiation, which suggests a different method of translation regulation.[64,67,106] The dephosphorylation of eIF2α triggered by a rapid, local increase in GADD34 levels could explain this and begs closer examination. Finally, our imaging studies suggest the presence of GADD34 in non-neuronal cells, mostly glia, and point to the possibility that GADD34 controls translation initiation in other brain cells. This observation requires more thorough investigation to increase our understanding of how eIF2-dependent translation is regulated in a cell-type-specific manner during plasticity in the brain.

Translational regulation of GADD34 expression in neurons

Historically, GADD34 expression has been associated with the ISR, where its transcription is elevated as a consequence of increased translation of ATF4/CREB2.[73,75] In contrast, GADD34 expression increases in neuroblastoma cells when stimulated for 6 h with a cannabinoid receptor agonist, which is reliant on CREB-dependent gene transcription.[82] Our findings are similar in that they demonstrate a stress-independent increase in GADD34 protein levels. However, our findings differ from the previous studies in neuroblastoma cells in that we found no differences in GADD34 mRNA levels. Instead, we found that the BDNF-induced increase in GADD34 levels is regulated at the translational level. A previous study found that *de novo* translation of GADD34 can be achieved through chemical LTP induction in acute hippocampal slices.[107] Nevertheless, it should be noted that there are differences in the temporal window for measuring GADD34, the extracellular stimuli

delivered, and the cell types utilized in the two studies, which could explain the mechanistic differences for how GADD34 levels are increased.

As mentioned above, most previous studies have examined GADD34 expression during conditions of cellular stress when its expression is mediated by ATF4 at the transcriptional level.[73,108,109] However, the GADD34 mRNA contains two uORFs, components of the 5′ UTRs of mRNAs that were originally described to negatively impact ribosome scanning of the coding sequence.[110,111] In fact, the second uORF presents a Pro-Pro-Gly motif juxtaposed to the stop codon, which is poorly translated and can thus induce ribosome stalling upstream to the coding sequence.[112-115] Substituting this motif by Ala-Ala-Ala releases the brake in GADD34 translation, and elevated expression can be found even under resting conditions.[110] Therefore, it is possible that BDNF triggers the release of this brake of ribosomes and translation reinitiation in neurons, which would explain the increase in GADD34 expression we observed in our experiments. In fact, ribosome footprinting analysis of neuronal transcripts revealed that uORF-containing mRNAs are actively translated in both soma and dendrites,[24] building on the challenging of the notion that uORFs only suppress translation.[74] In fact, *Ppp1r15a* mRNA contain two short uORFs, which are associated with a higher possibility of reinitiation of translation at the main ORF.[116-118] Additionally, we cannot exclude the possibility that *Ppp1r15a* mRNAs are stored in mRNA granules, membraneless structures present in dendrites and axons that contain quiescent ribosomes and mRNAs. Granule components can be rearranged after neuronal stimulation and trigger translation of these transcripts locally, ensuring a rapid response to activity.[119] The fact that we can identify *Ppp1r15a* mRNA in dendrites and that BDNF increases its association to polysomes supports this hypothesis. Nevertheless, more experiments are required to understand how exactly uORFs modulate *Ppp1r15a* mRNA translation and what type of control takes place in neurons.

GADD34 expression converges with cytoskeleton dynamics to promote eIF2α dephosphorylation

We found that BDNF can promote an increase in the interaction between GADD34 and actin, which acts as a stabilizer of the primary interaction between GADD34 and eIF2α. Our experiments suggest that this interaction relies on an increased availability of G-actin after neuronal stimulation, through decreased phosphorylated cofilin after exposure to BDNF. The role of cofilin during synaptic consolidation is controversial. Classically, LTP is associated with higher phosphorylation of cofilin and elevated levels of actin polymerization, a mechanism that appears to rely on protein synthesis.[120,121] On the other hand, the induction of LTD drives the opposite effect, with less phosphorylated cofilin and higher actin depolymerization.[122] This dichotomy was challenged by another report that described a massive translocation of active cofilin to the dendritic spine at early stages of LTP.[123] Previous reports suggested that cofilin is transiently dephosphorylated by the phosphatase slingshot 1 at early stages of synapse activation to sever F-actin and generate a source of G-actin.[124-126] Moreover, actin monomers are crucial for insertion of AMPA receptors (AMPA-Rs) at the surface of dendritic spines after LTP. In fact, dephosphorylated cofilin stimulates the integration of AMPA-Rs to the surface, whereas the phosphorylated version has the opposite effect.[127] Because eIF2α-P can influence the amounts of AMPA-R

present in the post-synaptic density,[29] and because we found that artificially increasing G-actin levels can promote GADD34-eIF2α interactions, it is possible that actin monomers increase AMPA-Rs at the synapse by promoting eIF2α dephosphorylation.

Our findings indicate that the overexpression of cofilin can promote neuronal protein synthesis, providing a link between the dynamic regulation of the cytoskeleton with an increase in translation. The interplay between actin dynamics and protein synthesis is critical for neuronal function[34-36,128] and, when unbalanced, appears to underlie neuronal dysfunction in fragile X syndrome (FXS). In FXS model mice, the lack of fragile X protein results in increased Rac1 activity, a GTPase that promotes actin remodeling and increases eIF4E-eIF4G interactions, thus potentiating *de novo* translation.[129] Here, we show an additional molecular pathway through which actin dynamics can regulate neuronal translation initiation by promoting the interaction between GADD34-eIF2α. The next step of investigation requires more detailed analysis of structural changes in actin in the dendritic spine and the consequences for local translation initiation at this subcellular structure.

In conclusion, our findings demonstrate a molecular pathway through which neurons can increase protein synthesis upon BDNF stimulation. This pathway relies on the release of a translational brake on GADD34, which in turn can bind to eIF2α-P in both soma and dendrites in a G-actin-dependent manner to promote *de novo* protein synthesis (Figure S7). These events culminate with the translation of mRNAs that encode proteins involved in synaptic plasticity. Our results open alternative avenues toward understanding the molecular mechanisms of translational control that underlie long-lasting changes in neuronal function that are induced by neuronal activity that contribute to memory formation and that are altered in cognitive disorders.

Limitations of the study

Although the results of these experiments are consistent with the literature and describe a complex mechanism for promoting translation initiation in response to neuronal stimulation, it is important to note that these experiments were performed entirely in primary neurons, which may differ when compared to mature neurons in a developed brain. Furthermore, the utilization of BDNF application to stimulate neurons limits the interpretations of the data when translating them to a cognitive phenomenon.

STAR★METHODS

RESOURCE AVAILABILITY

Lead contact—Further information and requests for resources and reagents should be directed to and will be fulfilled by the lead contact, Dr. Eric Klann (ek65@nyu.edu).

Materials availability—AAV9.EF1a.m.Cherry.SICO.shRNA-GADD34 is available upon reasonable request to the load contact, Dr. Eric Klann.

Data and code availability

- Access to original data - TRAP-seq and total RNA-seq datasets used on this manuscript are deposited on the Gene Expression Omnibus (GEO), under accession number GSE248013, and are freely available to all users.
- Access to original code - This paper does not report original code.
- Access to any additional information - Any additional information required to reanalyze the data reported in this work paper is available from the lead contact upon request.

EXPERIMENTAL MODEL AND STUDY PARTICIPANT DETAILS

Wild-type C57/bl6J and B6N.129P2(Cg)-*Ppp1r15*atm1.1Aif/Mmnc (GADD34$^{fl/fl}$ mice) *Mus musculus* were kept with food and water *ad libitum* and were maintained in a 12-12h light-dark cycle at stable temperature (78°F) and humidity (40–50%). All mice were back-crossed to the C57/Bl6j strain for at least five generations. Mice used for timed pregnancy were 10–16 weeks old. All procedures involving the use of animals were performed in accordance with the guidelines of the National Institutes of Health and were approved by the Institutional Animal Care and Use Committee (IACUC, protocol 06–1270) at New York University. Due to the nature of *in vitro* experiments, there was no discrimination between sexes of mouse embryos used for primary neuron preparations.

Primary neuron preparation and maintenance—E17 pregnant C57/Bl6J mice were obtained and euthanized by cervical dislocation. The embryos were removed from the vitellin sack and brains were extracted and kept on ice-cold HBSS +0.37% glucose. Cortico-hippocampal masses were isolated from the brain stem and cerebellum with use of blunted-end tweezers, and meninges were carefully removed, avoiding tissue puncturing. Tissue was kept on ice during the whole process. For chemical digestion, tissue was incubated for 5 min with 0.25% trypsin solution at 37°C. Trypsin was inactivated with two sequential washes with DMEM +10% FBS and 1% Pen/Strep. For mechanical isolation of cells, tissue was resuspended in supplemented DMEM and disrupted with fire-polished Pasteur glass pipettes (15 strokes). Cells then were centrifuged at 900 *g*/5 min/RT and carefully resuspended in Neurobasal supplemented with 2% B27, 1% Pen/Strep and 1% GlutaMax at 37°C. The total amount of cells in suspension was determined by manual count using a Neubauer chamber. For imaging analysis, cells were plated at a final density of 100,000 cells/well (24-well plates and 4-well culture slides) or 200,000 cells/well (12-well plates). For western blotting and polysome profiling analysis, cells were plated at a density of 2,000,000 cells/well (6-well plates) or 20,000,000 cells/well (Petri dishes). Cells were plated in glass coverslips or polypropylene plastic plates coated with a 0.1% poly-L-ornithine solution supplemented with 4 μg/mL of laminin. After 1 h, the Neurobasal was aspirated with vacuum from the wells and replaced with fresh Neurobasal, supplemented as above. Cells were always kept at 37°C/5% CO2 conditions, and 40% of media was replaced every three days with fresh Neurobasal, until *DIV* (days *in vitro*) 14, when cells were used for experimentation. For experiments with either BDNF or thapsigargin, cells were treated at the final day of culture with a final concentration of 50 ng/mL of BDNF or 1 μg/mL of thapsigargin (times of incubation are delineated in the figure legends). For puromycilation

and puro-PLA experiments, cells were exposed to 0.5 μg/mL of puromycin 5 min prior to fixation.

METHOD DETAILS

RNA scope—Cells were cultured in chambered slides and treated/fixed as described above. To perform fluorescent *in situ* hybridization, the protocol of the manufacturer was followed. Briefly, cells were permeabilized for 5 min using protease IV diluted 1:15, rinsed 3x in PBS. Hybridization was performed for 2 h at 40°C using ACD Bio HyBEZ oven. Cells were washed 2x with 1x RNA scope wash buffer, and then amplification was performed with the following conditions: AMP 1-FL for 30 min at 40°C, AMP 2-FL for 15 min at 40°C, AMP 3-FL for 30 min at 40°C and AMP 4-FL for 30 min at 40°C. Between each amplification step, cells were washed twice with 1x RNA scope wash buffer. After RNA scope, immunostaining was performed. Cells were blocked with 5% normal goat serum solution and incubated for 30 min at room temperature with anti-MAP2 antibody. Cells were washed 2x with 1x RNA scope buffer and incubated with secondary anti-chicken for 30 min at room temperature. Cells were washed again 2x with RNA scope buffer, rinsed in Mili-q water and mounted using Antifade Prolong mounting media + DAPI.

Immunocytochemistry—After treatment, Neurobasal was aspired with a vacuum and briefly rinsed with pre-warmed PBS. PBS was aspired and cells were fixed for 20 min with PBS +4% paraformaldehyde (PFA) + 4% sucrose solution at RT. Fixative solution was removed and cells were rinsed 4x with PBS. For permeabilization, neurons were incubated for 15 min/RT with PBS +0.5% Triton X-100 and rinsed twice with PBS. The coverslips then were incubated for 1 h with blocking solution consisting of 5% NGS in PBS and then incubated overnight/4°C with primary antibodies diluted in blocking solution. The next day, cells were washed 3 × 5 min with PBS and incubated for 1 h at room temperature with secondary antibodies diluted in blocking solution, then washed 3 × 5 min with PBS again. Coverslips were mounted on Prolong + DAPI, when 405 channel was available for DAPI staining. Otherwise, Prolong without DAPI was used instead. Slides were incubated for 24 h at room temperature to dry mounting media before imaging. The concentrations of the primary and secondary antibodies are shown in Table 1. Imaging was done using a Leica SP8 Confocal microscope within a week after finishing immunocytochemistry. 40X or 63 × magnification objective were used, and 10–15 z-stacks were obtained per image, separated by 0.5 mm. Images were obtained at a final resolution of 512 x 512 pixels.

Western blotting—Cells were scraped from the plate in cold RIPA buffer (10 mM Tris-Cl pH8.0, 1 mM EDTA, 1% Triton X-100, 0.1% sodium deoxycolate, 0.1% SDS, 140 mM NaCl) and flash frozen on dry ice. The resulting lysates were sonicated and cleared through centrifugation (10.000 *g*/10 min/4°C). Supernatant was transferred to a new tube and total protein mass was quantified using BCA kit. Samples were prepared in Laemmli buffer supplemented with 10 mM DTT and boiled at 95°C for 3 min. After cooling to room temperature, samples were spun and applied in 4–20% Tris-Glycine electrophoresis gels to a final mass of 20–40 μg of protein per lane, depending on the experiment performed. Proteins were separated at a fixed voltage of 100V, and then transferred to polyvinylidene difluoride (PVDF) membranes using iBlot2 apparatus (23V/6 min). Membranes then were

incubated with 5% milk for 30 min, then 5% BSA for 30 min. Membranes were incubated with primary antibodies diluted in 5% BSA at 4°C/overnight/rocking, and then washed 3x with TBS +0.1% Tween 20 (TBS-T). Membranes were incubated with secondary antibodies diluted in 5% BSA for 1 h at room temperature while rocking, and then washed 3x with TBS-T and 3x with TBS. Development was done with use of ECL kits from Amersham/GE, using a Protein Simple apparatus (Kodak). For quantitative analysis, Fiji was used. First, background was subtracted, then a densitometry analysis was performed to quantify band sizes. As a loading control, β-actin band intensity was used. To obtain normalized values, band intensities of proteins of interest were divided by the band density of β-actin. All samples from control group (e.g., vehicle or wild-type) were averaged to obtain a value, defined as 100%. The total percentage of each experimental point was then obtained by using 100% as reference.

Polysome profiling—Cultured mouse cortical neurons at DIV 14 were treated with either vehicle or BDNF (50 ng/mL) for 1 h. Neurons then were treated with cycloheximide (CHX) at 100 μg/mL for 1 min at 37°C. After washing twice with phosphate buffered saline with 100 μg/mL CHX-treated cells we scraped in polysome buffer (20 mM Tris pH 7.5, 150 mM NaCl, 5 mM $MgCl_2$, 100 μg/mL cycloheximide, 1 mM DTT) and centrifuged at 300 *g*/5 min/4°C in a swing bucket rotor. Pellets were lysed using polysome lysis buffer (20 mM Tris pH 7.5, 150 mM NaCl, 5 mM $MgCl_2$, 1% Triton X-100, 24 U/ml Turbo DNase, 100 U/ml RNasin Plus, 100 μg/mL cycloheximide, 1 mM DTT, protease inhibitor cocktail, and 8% glycerol) and the lysate was triturated with 23-gauge syringe, followed by centrifugation 16.100*g*/10 min/4°C. Samples then were loaded onto 14 mL 10 to 50% sucrose gradients prepared in polysome buffer (20 mM Tris pH 7.5, 150 mM NaCl, 5 mM MgCl2, 100 μg/mL cycloheximide, 1 mM DTT, 100U/ml RNasin Plus, and 8% glycerol) and centrifuged for 2 h 45 min at 36,000 revolutions per minute (rpm) at 4°C in an SW41 Ti swing-out rotor. Polysome profiling was carried out using a Piston Gradient Fractionator (Biocomp) with continuous monitoring at 254 nm using a Model EM-1 Econo UV detector (BioRad). Monosome and polysome fractions of approximately 400 μL were collected with a fraction collector (Gilson FC203B).

RNA purification and RT-PCR—TRAP and total lysate RNA were isolated via the RNeasy Plus Kit (Qiagen). The samples were first lysed and homogenized in Buffer RLT Plus. The lysates then were centrifuged through a gDNA Eliminator spin column for 30 s. The flow through was saved and 300 μL of 70% ethanol was added. The sample was then passed through the RNeasy spin column for 15 s. RNA bound to the membrane and the contaminants were washed away. The RNA in the spin column membrane was washed in 700 μL of buffer RW1 and 1000 μL of buffer RPE. The isolated RNA was eluted in 30 μL of RNase free water. The concentration of RNA for each sample was determined using Tapestation (Agilent) and was later normalized to 10 ng/μL. The RNA expression levels of the target mRNA *Ppp1r15a* along with an endogenous control gene, *Gapdh,* were measured in a qPCR reaction. The qPCR reactions were performed using the Luna Universal One-Step RT-qPCR kit. For each reaction, 19 μL of a qPCR master mix containing Luna Universal One-Step Reaction mix, Luna WarmStart RT Enzyme mix, Forward Primer, Reverse Primer, and Nuclease-free water was added to a 96 well plate. 1 μL of the 10 ng RNA sample was

then added to the 96 well plate, and 1 μL of RNase free water was used as the negative control. Technical replicate qPCR reactions were run on the same plate. Next, the qPCR reactions were run using SYBR fluorescence on a BioRad CFX96 qPCR cycler. Following the qPCR reactions, the threshold values (Ct) were used to calculate the fold change. First, the Ct value of the endogenous control was subtracted from the Ct value of the target gene to determine the target ΔCt. ($Target\,\Delta Ct = Ct_{GADD34} - Ct_{GAPDH}$). The average ΔCts from all three of the technical replicates was then calculated along with the average ΔCts from the negative control. The negative control average ΔCt values then were subtracted from the target ΔCt values giving a ΔΔCt value ($\Delta\Delta Ct = \Delta Ct_{Target} - \Delta Ct_{NTC}$). Finally, to determine the fold change, 2 was raised to the negative ΔΔCt (Fold Changes = $2^{-\Delta\Delta Ct}$). For the polysome profiling fraction qPCRs, RNA collected from polysome profiling experiments was isolated from the sucrose gradient via the Direct-zol RNA MiniPrep Kits (Zymo). The RNAs from each fraction were lysed and homogenized in 400 μL TRI-Reagent (Zymo). An equal volume of 95–100% ethanol was added to the lysed samples and thoroughly mixed. The mixture then was transferred to a Zymo-spin IICR Column and centrifuged. The RNA bound to the spin column membrane and the flow through was discarded. The spin column was washed with 800 μL of RNA Pre-wash and 700 μL of RNA wash buffer. The RNA then was eluted in 30 μL of nuclease-free water. The concentration for each RNA fraction was determined using Tapestation (Agilent) and later normalized to 10 ng/μL. RT-qPCR reactions were performed as described previously.

Proximity ligand assays—Cells were rinsed, fixed, and blocked as described above. Proximity Ligand Assays (PLA) were performed following instructions from the manufacturer. Briefly, cells were incubated with either a combination of anti-GADD34 (rabbit)/anti-eIF2α (mouse), anti-GADD34 (rabbit)/anti-actin (mouse), anti-GADD34 (rabbit)/anti-puromycin (mouse) or anti-eIF2αP (rabbit) overnight/4°C. In all experiments, cells were also incubated with anti-MAP2 (chicken) and, when transduced with viruses, anti-mCherry (rat). Cells were washed 3 × 5 min with PBS and incubated at 37°C for 1 h with PLA probes (rabbit or mouse) diluted 1:5 in blocking buffer, and secondary anti-Chk (1:500). Cells were washed 4x5 min/RT with 1x PLA buffer A. Cells then were incubated at 37°C for 30 min with ligase diluted in 1x PLA ligase buffer, and subsequently washed 4 × 5 min at room temperature with 1x PLA buffer A. Finally, for amplification, cells were incubated at 37°C for 100 min with polymerase diluted in 1x PLA amplification buffer and rinsed twice with buffer B at room temperature. Cells then were washed 2 × 10 min at room temperature with buffer B, 3 × 5 min with PBS and mounted with Prolong + DAPI. After the mounting media was dry, cells were immediately imaged using a Leica SP8 Confocal microscope. A 40× magnification objective was used, and stacks were obtained separated by 0.2 μm (25–40 stacks per image). Images were obtained at a final resolution of 1024 x 1024 pixels.

Translating ribosome affinity purification (TRAP)—On the day before sample collection, the affinity matrix (composed of protein L-coated magnetic beads + anti-GFP antibodies) was prepared. Briefly, MyOne T1 Dynabeads were incubated for 30 min with 120 μg of protein L at RT, rotating. Beads were washed 5x with RNAse-free PBS +3% protease and IgG-free BSA and incubated with 50 μg of each anti-GFP antibody (19C8

and 19F7) for 1h/RT/rotating. Beads were washed 3x with low-salt buffer (20 mM HEPES KOH pH 7.3, 150 mM KCl, 10 mM $MgCl_2$, 1 % NP-40, 0.5 mM DTT, 100 μg/mL Cycloheximide and protease/phosphatase inhibitor) and stored until use. On the next day, samples from neurons treated for 1 h with either vehicle or 50 ng/mL BDNF were collected. Prior to sample collection, neurons were exposed to 100 μg/mL cycloheximide for 1 min to block translation. Cells were washed 3x with ice-cold RNAse-free PBS +100 μg/mL cycloheximide on ice, and gently scraped in cell lysis buffer (100 mM HEPES KOH pH 7.3, 750 mM KCl, 50 mM $MgCl_2$, 1 % NP-40,0.5 mM DTT, 40 units/ml RNAsin, 20 units/ml Superasin, 100 μg/mL cycloheximide and protease/phosphatase inhibitor). The lysates were transferred to a pre-chilled glass homogenizer and 12 strokes were performed with an automatic pestle, avoiding sample aeration. Cell lysates were transferred to pre-chilled 1.5 mL RNAse-free tubes and centrifuged at 2000 *g*/10min/4°C. The supernatant was transferred to a new tube and supplemented with 1/9th of the volume of 300 mM DHPC solution (e.g., 111 μL for every ml of sample). Samples were homogenized by inversion and incubated for 5 min on ice, followed by new centrifugation at 20,000 *g*/10min/4°C. Supernatant was collected and incubated at 200 μL of affinity matrix/sample overnight/4°C/rotating. On the next day, beads were isolated using a magnet, and washed 4x with high-salt buffer (20 mM HEPES KOH pH 7.3, 350 mM KCl, 10 mM $MgCl_2$, 1 % NP-40, 0.5 mM DTT, 100 μg/mL cycloheximide and protease/phosphatase inhibitor). After the last wash, buffer was removed, and beads were allowed to return to room temperature before adding 300 μL of lysis buffer from RNEasy Miniprep Plus kit supplemented with β-mercaptoethanol. Samples were incubated for 10 min at room temperature to allow elution, and beads were removed magnetically, and supernatant transferred to a new tube.

RNA sequencing—TRAP was performed as described above. Quality control of both total RNA and purified RNA was measured using Agilent HS TapeStation. cDNA then was synthesized with Takara SMART-Seq HT kit with 1 ng of RNA input that had RIN of 5 and greater via Agilent HS TapeStation. Libraries were constructed with 0.25 ng of cDNA input via Nextera XT DNA library kit. cDNA and libraries amplification had both 12 cycles. Quality control of libraries were analyzed via Agilent HS TapeStation and Invitrogen Quant-it. Samples were pooled at equal molarity before sequencing. Final libraries were sequenced paired-end 50 cycles on an Illumina NovaSeq6000 S1 100 cycle Flow Cell-v1.5 with 1% Phix spike-in.

Bioinformatics—For alignment of Fastq files, sequencing adapters and low-quality bases were trimmed using Cutadapt version 1.8.2 using the following arguments (-q 20 -O 1 -a CTGTCTCTTATA).[132] Trimmed reads were then aligned to the mouse genome (mm10) using STAR version 2.7.7a[137] and raw gene counts were obtained using the argument (*−quantmode*).

After alignment, a count matrix was generated using scripts generated in house. The count matrix was batch normalized using ComBat-Seq,[133] and used as input for DESeq2 package for differential expression analysis.[134] In the analysis design, both genotype (WT vs. KO) and treatment (vehicle vs. BDNF) were included. Data was transformed using variance stabilizing transformations (vst) and used as input for PCA. For the PCA, the

plotPCA function (imbued in the DESeq package) was used. For unsupervised clustering, the DESeq object generated was transformed into a matrix, which then was used to calculate a correlational matrix between samples. Heatmaps were generated using pHeatmap package. Log_2 fold changes were retrieved using lfcShrink function, using "apelgm" as an estimator.[138] To obtain a list of significant DEGs, the list of genes was subset for FDR < 0.1.[139]

Gene Ontology analysis was performed using clusterProfiler package.[136] Briefly, the list of significantly upregulated or downregulated DEGs were transformed into ENSEMBL IDs using bitr function, and the list was queried against a background list, that consisted of all genes identified on the sequencing. All GO types were analyzed together, with a p value cutoff of 0.05. The p value was adjusted using Benjamin & Hochberg's method. GOs included in figures were selected based on (1) significance; and (2) groups of interest. synGO analysis[140] was performed using the official repository (www.syngoportal.org) using standard methods.

G/F-actin ratio experiments—After cells were treated with either vehicle or BDNF, cell lysates were scraped in ice-cold "G-actin buffer" (10 mM $KHPO_4$, 50 mM KCl, 2 mM $MgCl_2$, 1 mM EGTA, 0.2 mM DTT, 0.5% Triton X-100, 1 mM sucrose and 100 mM NaF, supplemented with protease/phosphatase inhibitors). Lysates were kept ice-cold through the whole process. Cell lysates were sonicated and spun at 15.000 *g*/30 min/4°C. Supernatant, containing G-actin, was saved and frozen until use. The pellet was resuspended in ice-cold F-actin buffer (1.5 mM guanidine hydrochloride, 1 mM sodium acetate, 1 mM $CaCl_2$,1 mM ATP and 20 mM Tris-HCl pH 7.4, supplemented with protease/phosphatase inhibitors) and sonicated again. Lysates were centrifugated at 15,000 *g*/30 min/4°C and supernatant containing F-actin was saved. Protein samples were quantified and loaded on tris-glycine gels, as described above. A Western blot using anti-pan-actin as the primary antibody was performed to develop the total levels of actin in each sample.[129]

QUANTIFICATION AND STATISTICAL ANALYSIS

Image analysis—All fluorescence intensity, PLA, RNA scope and Western blot band density analysis were performed using Fiji (ImageJ). For fluorescence intensity and RNA scope, the channel containing MAP2 (a neuronal marker), GFP or mCherry (when neurons were transduced with viral constructs) was initially isolated and used as template for a mask to define the region of interest (i.e., neuronal area). This mask was applied over the channel containing the staining of interest, and a threshold was applied to separate real signal from noise, using staining performed with no primary antibodies as background. The integrated density was then obtained and normalized by the total neuronal area. For PLA, an ImageJ-based script developed by Heumuller and colleagues[33] was kindly provided by Dr. Erin Schuman and used to calculate total intensity of punctate signal. For western blots, the bands were straightened using rotation tool and then total staining density was calculated using the raw integrated density parameter in Fiji. For every image analysis, the experimenter was blind to all conditions. No parameters of brightness or contrast were altered prior to quantification.

Data analysis—Data analysis and plotting were performed using GraphPad Prism (v9). Details regarding the tests used and the number of technical and biological replicates for each experiment are described in figure legends. For all Western blotting experiments, every biological replicate contained one representative of each experimental condition. Given that, paired analysis was used to measure statistical significance, to avoid batch effects-derived bias (i.e., natural fluctuations on protein expression resulting from biological replicate heterogeneity). Unpaired analysis were used to analyze immunofluorescence, RNA Scope and PLAs. When three independent conditions were analyzed together, One-Way ANOVA was performed. When two interacting conditions (i.e., genotype vs. treatment) were analyzed, two-Way ANOVA was performed. For time course data, One-Way ANOVA repeated measures was performed. All graphics display minimum to maximum value, with median represented as a black line in the barplot. Data normality was visualized using Q-Q plots before appropriate statistical test application. Outliers were excluded from the analysis using the Grubb's test ($\alpha = 0.05$) after all experimental data was collected.

Supplementary Material

Refer to Web version on PubMed Central for supplementary material.

ACKNOWLEDGMENTS

We would like to thank Dr. Erin Schuman and Dr. Georgi Tushev for insightful comments and for the donation of the metagene plot included in the manuscript. We are grateful to Claudia Farb for her technical assistance. This study was funded by NIH, grant NS122316.

REFERENCES

1. Flexner LB, Flexner JB, Roberts RB, and Delahaba G (1964). Loss of Recent Memory in Mice as Related to Regional Inhibition of Cerebral Protein Synthesis. Proc. Natl. Acad. Sci. USA 52, 1165–1169. [PubMed: 14231435]
2. Oliveira MM, and Klann E (2022). eIF2-dependent translation initiation: Memory consolidation and disruption in Alzheimer's disease. Semin. Cell Dev. Biol 125, 101–109. [PubMed: 34304995]
3. Cheng W, Wang S, Mestre AA, Fu C, Makarem A, Xian F, Hayes LR, Lopez-Gonzalez R, Drenner K, Jiang J, et al. (2018). C9ORF72 GGGGCC repeat-associated non-AUG translation is upregulated by stress through eIF2alpha phosphorylation. Nat. Commun 9, 51. [PubMed: 29302060]
4. Chou A, Krukowski K, Jopson T, Zhu PJ, Costa-Mattioli M, Walter P, and Rosi S (2017). Inhibition of the integrated stress response reverses cognitive deficits after traumatic brain injury. Proc. Natl. Acad. Sci. USA 114, E6420–E6426. [PubMed: 28696288]
5. Evans HT, Benetatos J, van Roijen M, Bodea LG, and Götz J (2019). Decreased synthesis of ribosomal proteins in tauopathy revealed by non-canonical amino acid labelling. EMBO J. 38, e101174. [PubMed: 31268600]
6. Evans HT, Taylor D, Kneynsberg A, Bodea LG, and Götz J (2021). Altered ribosomal function and protein synthesis caused by tau. Acta Neuropathol. Commun 9, 110. [PubMed: 34147135]
7. Lourenco MV, Clarke JR, Frozza RL, Bomfim TR, Forny-Germano L, Batista AF, Sathler LB, Brito-Moreira J, Amaral OB, Silva CA, et al. (2013). TNF-alpha mediates PKR-dependent memory impairment and brain IRS-1 inhibition induced by Alzheimer's beta-amyloid oligomers in mice and monkeys. Cell Metabol. 18, 831–843.
8. Lourenco MV, Ferreira ST, and De Felice FG (2015). Neuronal stress signaling and eIF2alpha phosphorylation as molecular links between Alzheimer's disease and diabetes. Prog. Neurobiol 129, 37–57. [PubMed: 25857551]

9. Ma T, Trinh MA, Wexler AJ, Bourbon C, Gatti E, Pierre P, Cavener DR, and Klann E (2013). Suppression of eIF2alpha kinases alleviates Alzheimer's disease-related plasticity and memory deficits. Nat. Neurosci 16, 1299–1305. [PubMed: 23933749]
10. Oliveira MM, Lourenco MV, Longo F, Kasica NP, Yang W, Ureta G, Ferreira DDP, Mendonça PHJ, Bernales S, Ma T, et al. (2021). Correction of eIF2-dependent defects in brain protein synthesis, synaptic plasticity, and memory in mouse models of Alzheimer's disease. Sci. Signal 14, eabc5429. [PubMed: 33531382]
11. Wong YL, LeBon L, Basso AM, Kohlhaas KL, Nikkel AL, Robb HM, Donnelly-Roberts DL, Prakash J, Swensen AM, Rubinstein ND, et al. (2019). eIF2B activator prevents neurological defects caused by a chronic integrated stress response. Elife 8, e42940. [PubMed: 30624206]
12. Santini E, Huynh TN, MacAskill AF, Carter AG, Pierre P, Ruggero D, Kaphzan H, and Klann E (2013). Exaggerated translation causes synaptic and behavioural aberrations associated with autism. Nature 493, 411–415. [PubMed: 23263185]
13. Zhu PJ, Khatiwada S, Cui Y, Reineke LC, Dooling SW, Kim JJ, Li W, Walter P, and Costa-Mattioli M (2019). Activation of the ISR mediates the behavioral and neurophysiological abnormalities in Down syndrome. Science 366, 843–849. [PubMed: 31727829]
14. Arora A, Castro-Gutierrez R, Moffatt C, Eletto D, Becker R, Brown M, Moor AE, Russ HA, and Taliaferro JM (2022). High-throughput identification of RNA localization elements in neuronal cells. Nucleic Acids Res. 50, 10626–10642. [PubMed: 36107770]
15. Arora A, Goering R, Lo HYG, Lo J, Moffatt C, and Taliaferro JM (2021). The Role of Alternative Polyadenylation in the Regulation of Sub-cellular RNA Localization. Front. Genet 12, 818668. [PubMed: 35096024]
16. Engel KL, Arora A, Goering R, Lo HYG, and Taliaferro JM (2020). Mechanisms and consequences of subcellular RNA localization across diverse cell types. Traffic 21, 404–418. [PubMed: 32291836]
17. Martin KC, and Ephrussi A (2009). mRNA localization: gene expression in the spatial dimension. Cell 136, 719–730. [PubMed: 19239891]
18. Taliaferro JM (2022). Transcriptome-scale methods for uncovering subcellular RNA localization mechanisms. Biochim. Biophys. Acta Mol. Cell Res 1869, 119202. [PubMed: 34998919]
19. Chekulaeva M. (2023). First demonstration of miRNA-dependent mRNA decay. Nat. Rev. Mol. Cell Biol 24, 164.
20. Mendonsa S, von Kügelgen N, Dantsuji S, Ron M, Breimann L, Baranovskii A, Lödige I, Kirchner M, Fischer M, Zerna N, et al. (2023). Massively parallel identification of mRNA localization elements in primary cortical neurons. Nat. Neurosci 26, 394–405. [PubMed: 36646877]
21. Sun C, and Schuman EM (2022). Logistics of neuronal protein turnover: Numbers and mechanisms. Mol. Cell. Neurosci 123, 103793. [PubMed: 36396040]
22. Cajigas IJ, Tushev G, Will TJ, tom Dieck S, Fuerst N, and Schuman EM (2012). The local transcriptome in the synaptic neuropil revealed by deep sequencing and high-resolution imaging. Neuron 74, 453–466. [PubMed: 22578497]
23. Biever A, Glock C, Tushev G, Ciirdaeva E, Dalmay T, Langer JD, and Schuman EM (2020). Monosomes actively translate synaptic mRNAs in neuronal processes. Science 367, eaay4991. [PubMed: 32001627]
24. Glock C, Biever A, Tushev G, Nassim-Assir B, Kao A, Bartnik I, Tom Dieck S, and Schuman EM (2021). The translatome of neuronal cell bodies, dendrites and axons. Proc. Natl. Acad. Sci. USA 118. e2113929118. [PubMed: 34670838]
25. Tushev G, Glock C, Heumüller M, Biever A, Jovanovic M, and Schuman EM (2018). Alternative 3' UTRs Modify the Localization, Regulatory Potential, Stability, and Plasticity of mRNAs in Neuronal Compartments. Neuron 98, 495–511.e6. [PubMed: 29656876]
26. Hafner AS, Donlin-Asp PG, Leitch B, Herzog E, and Schuman EM (2019). Local protein synthesis is a ubiquitous feature of neuronal pre- and postsynaptic compartments. Science 364, eaau3644. [PubMed: 31097639]
27. Donlin-Asp PG, Polisseni C, Klimek R, Heckel A, and Schuman EM (2021). Differential regulation of local mRNA dynamics and translation following long-term potentiation and depression. Proc. Natl. Acad. Sci. USA 118, e2017578118. [PubMed: 33771924]

28. Ostroff LE, Santini E, Sears R, Deane Z, Kanadia RN, LeDoux JE, Lhakhang T, Tsirigos A, Heguy A, and Klann E (2019). Axon TRAP reveals learning-associated alterations in cortical axonal mRNAs in the lateral amgydala. Elife 8, e51607. [PubMed: 31825308]
29. Di Prisco GV, Huang W, Buffington SA, Hsu CC, Bonnen PE, Placzek AN, Sidrauski C, Krnjević K, Kaufman RJ, Walter P, and Costa-Mattioli M (2014). Translational control of mGluR-dependent long-term depression and object-place learning by eIF2alpha. Nat. Neurosci 17, 1073–1082. [PubMed: 24974795]
30. Mockett BG, Guévremont D, Elder MK, Parfitt KD, Peppercorn K, Morrissey J, Singh A, Hintz TJ, Kochen L, Tom Dieck S, et al. (2019). Glutamate Receptor Trafficking and Protein Synthesis Mediate the Facilitation of LTP by Secreted Amyloid Precursor Protein-Alpha. J. Neurosci 39, 3188–3203. [PubMed: 30804097]
31. Lopez J, Gamache K, Schneider R, and Nader K (2015). Memory retrieval requires ongoing protein synthesis and NMDA receptor activity-mediated AMPA receptor trafficking. J. Neurosci 35, 2465–2475. [PubMed: 25673841]
32. Snyder EM, Philpot BD, Huber KM, Dong X, Fallon JR, and Bear MF (2001). Internalization of ionotropic glutamate receptors in response to mGluR activation. Nat. Neurosci 4, 1079–1085. [PubMed: 11687813]
33. Heumüller M, Glock C, Rangaraju V, Biever A, and Schuman EM (2019). A genetically encodable cell-type-specific protein synthesis inhibitor. Nat. Methods 16, 699–702. [PubMed: 31308551]
34. Fifková E, Anderson CL, Young SJ, and Van Harreveld A (1982). Effect of anisomycin on stimulation-induced changes in dendritic spines of the dentate granule cells. J. Neurocytol 11, 183–210. [PubMed: 6279784]
35. Tanaka JI, Horiike Y, Matsuzaki M, Miyazaki T, Ellis-Davies GCR, and Kasai H (2008). Protein synthesis and neurotrophin-dependent structural plasticity of single dendritic spines. Science 319, 1683–1687. [PubMed: 18309046]
36. Yang Y, Wang XB, Frerking M, and Zhou Q (2008). Spine expansion and stabilization associated with long-term potentiation. J. Neurosci 28, 5740–5751. [PubMed: 18509035]
37. Wong HHW, Lin JQ, Ströhl F, Roque CG, Cioni JM, Cagnetta R, Turner-Bridger B, Laine RF, Harris WA, Kaminski CF, and Holt CE (2017). RNA Docking and Local Translation Regulate Site-Specific Axon Remodeling In Vivo. Neuron 95, 852–868.e8. [PubMed: 28781168]
38. Cioni JM, Koppers M, and Holt CE (2018). Molecular control of local translation in axon development and maintenance. Curr. Opin. Neurobiol 51, 86–94. [PubMed: 29549711]
39. Shigeoka T, Koppers M, Wong HHW, Lin JQ, Cagnetta R, Dwivedy A, de Freitas Nascimento J, van Tartwijk FW, Ströhl F, Cioni JM, et al. (2019). On-Site Ribosome Remodeling by Locally Synthesized Ribosomal Proteins in Axons. Cell Rep. 29, 3605–3619.e10. [PubMed: 31825839]
40. Piper M, Lee AC, van Horck FPG, McNeilly H, Lu TB, Harris WA, and Holt CE (2015). Differential requirement of F-actin and microtubule cytoskeleton in cue-induced local protein synthesis in axonal growth cones. Neural Dev. 10, 3. [PubMed: 25886013]
41. Koppers M, Cagnetta R, Shigeoka T, Wunderlich LC, Vallejo-Ramirez P, Qiaojin Lin J, Zhao S, Jakobs MA, Dwivedy A, Minett MS, et al. (2019). Receptor-specific interactome as a hub for rapid cue-induced selective translation in axons. Elife 8, e48718. [PubMed: 31746735]
42. Shigeoka T, Jung H, Jung J, Turner-Bridger B, Ohk J, Lin JQ, Amieux PS, and Holt CE (2016). Dynamic Axonal Translation in Developing and Mature Visual Circuits. Cell 166, 181–192. [PubMed: 27321671]
43. Cagnetta R, Wong HHW, Frese CK, Mallucci GR, Krijgsveld J, and Holt CE (2019). Noncanonical Modulation of the eIF2 Pathway Controls an Increase in Local Translation during Neural Wiring. Mol. Cell 73, 474–489.e5. [PubMed: 30595434]
44. Zhang X.h., and Poo MM (2002). Localized synaptic potentiation by BDNF requires local protein synthesis in the developing axon. Neuron 36, 675–688. [PubMed: 12441056]
45. Younts TJ, Monday HR, Dudok B, Klein ME, Jordan BA, Katona I, and Castillo PE (2016). Presynaptic Protein Synthesis Is Required for Long-Term Plasticity of GABA Release. Neuron 92, 479–492. [PubMed: 27764673]

46. Jung J, Ohk J, Kim H, Holt CE, Park HJ, and Jung H (2023). mRNA transport, translation, and decay in adult mammalian central nervous system axons. Neuron 111, 650–668.e4. [PubMed: 36584679]
47. Hartmann M, Heumann R, and Lessmann V (2001). Synaptic secretion of BDNF after high-frequency stimulation of glutamatergic synapses. EMBO J. 20, 5887–5897. [PubMed: 11689429]
48. Kolarow R, Brigadski T, and Lessmann V (2007). Postsynaptic secretion of BDNF and NT-3 from hippocampal neurons depends on calcium calmodulin kinase II signaling and proceeds via delayed fusion pore opening. J. Neurosci 27, 10350–10364. [PubMed: 17898207]
49. Kanhema T, Dagestad G, Panja D, Tiron A, Messaoudi E, Håvik B, Ying SW, Nairn AC, Sonenberg N, and Bramham CR (2006). Dual regulation of translation initiation and peptide chain elongation during BDNF-induced LTP in vivo: evidence for compartment-specific translation control. J. Neurochem 99, 1328–1337. [PubMed: 17064361]
50. Kelleher RJ 3rd, Govindarajan A, Jung HY, Kang H, and Tonegawa S (2004). Translational control by MAPK signaling in long-term synaptic plasticity and memory. Cell 116, 467–479. [PubMed: 15016380]
51. Takei N, Kawamura M, Ishizuka Y, Kakiya N, Inamura N, Namba H, and Nawa H (2009). Brain-derived neurotrophic factor enhances the basal rate of protein synthesis by increasing active eukaryotic elongation factor 2 levels and promoting translation elongation in cortical neurons. J. Biol. Chem 284, 26340–26348. [PubMed: 19625250]
52. Schratt GM, Nigh EA, Chen WG, Hu L, and Greenberg ME (2004). BDNF regulates the translation of a select group of mRNAs by a mammalian target of rapamycin-phosphatidylinositol 3-kinase-dependent pathway during neuronal development. J. Neurosci 24, 7366–7377. [PubMed: 15317862]
53. Smart FM, Edelman GM, and Vanderklish PW (2003). BDNF induces translocation of initiation factor 4E to mRNA granules: evidence for a role of synaptic microfilaments and integrins. Proc. Natl. Acad. Sci. USA 100, 14403–14408. [PubMed: 14623964]
54. Zhou X, Lin DS, Zheng F, Sutton MA, and Wang H (2010). Intracellular calcium and calmodulin link brain-derived neurotrophic factor to p70S6 kinase phosphorylation and dendritic protein synthesis. J. Neurosci. Res 88, 1420–1432. [PubMed: 20029971]
55. Huang YWA, Ruiz CR, Eyler ECH, Lin K, and Meffert MK (2012). Dual regulation of miRNA biogenesis generates target specificity in neurotrophin-induced protein synthesis. Cell 148, 933–946. [PubMed: 22385959]
56. Kang H, and Schuman EM (1996). A requirement for local protein synthesis in neurotrophin-induced hippocampal synaptic plasticity. Science 273, 1402–1406. [PubMed: 8703078]
57. Messaoudi E, Ying SW, Kanhema T, Croll SD, and Bramham CR (2002). Brain-derived neurotrophic factor triggers transcription-dependent, late phase long-term potentiation in vivo. J. Neurosci 22, 7453–7461. [PubMed: 12196567]
58. Ying SW, Futter M, Rosenblum K, Webber MJ, Hunt SP, Bliss TVP, and Bramham CR (2002). Brain-derived neurotrophic factor induces long-term potentiation in intact adult hippocampus: requirement for ERK activation coupled to CREB and upregulation of Arc synthesis. J. Neurosci 22, 1532–1540. [PubMed: 11880483]
59. Levine ES, Dreyfus CF, Black IB, and Plummer MR (1995). Brain-derived neurotrophic factor rapidly enhances synaptic transmission in hippocampal neurons via postsynaptic tyrosine kinase receptors. Proc. Natl. Acad. Sci. USA 92, 8074–8077. [PubMed: 7644540]
60. Li YX, Zhang Y, Lester HA, Schuman EM, and Davidson N (1998). Enhancement of neurotransmitter release induced by brain-derived neurotrophic factor in cultured hippocampal neurons. J. Neurosci 18, 10231–10240. [PubMed: 9852560]
61. Dean C, Liu H, Dunning FM, Chang PY, Jackson MB, and Chapman ER (2009). Synaptotagmin-IV modulates synaptic function and long-term potentiation by regulating BDNF release. Nat. Neurosci 12, 767–776. [PubMed: 19448629]
62. Rex CS, Lin CY, Kramár EA, Chen LY, Gall CM, and Lynch G (2007). Brain-derived neurotrophic factor promotes long-term potentiation-related cytoskeletal changes in adult hippocampus. J. Neurosci 27, 3017–3029. [PubMed: 17360925]

63. Shrestha P, and Klann E (2022). Spatiotemporally resolved protein synthesis as a molecular framework for memory consolidation. Trends Neurosci. 45, 297–311. [PubMed: 35184897]
64. Ostroff LE, Botsford B, Gindina S, Cowansage KK, LeDoux JE, Klann E, and Hoeffer C (2017). Accumulation of Polyribosomes in Dendritic Spine Heads, But Not Bases and Necks, during Memory Consolidation Depends on Cap-Dependent Translation Initiation. J. Neurosci 37, 1862–1872. [PubMed: 28087764]
65. Genheden M, Kenney JW, Johnston HE, Manousopoulou A, Garbis SD, and Proud CG (2015). BDNF stimulation of protein synthesis in cortical neurons requires the MAP kinase-interacting kinase MNK1. J. Neurosci 35, 972–984. [PubMed: 25609615]
66. Moon IS, Cho SJ, Seog DH, and Walikonis R (2009). Neuronal activation increases the density of eukaryotic translation initiation factor 4E mRNA clusters in dendrites of cultured hippocampal neurons. Exp. Mol. Med 41, 601–610. [PubMed: 19381064]
67. Gindina S, Botsford B, Cowansage K, LeDoux J, Klann E, Hoeffer C, and Ostroff L (2021). Upregulation of eIF4E, but not other translation initiation factors, in dendritic spines during memory formation. J. Comp. Neurol 529, 3112–3126. [PubMed: 33864263]
68. Gordiyenko Y, Schmidt C, Jennings MD, Matak-Vinkovic D, Pavitt GD, and Robinson CV (2014). eIF2B is a decameric guanine nucleotide exchange factor with a gamma2epsilon2 tetrameric core. Nat. Commun 5, 3902. [PubMed: 24852487]
69. Kashiwagi K, Ito T, and Yokoyama S (2017). Crystal structure of eIF2B and insights into eIF2-eIF2B interactions. FEBS J. 284, 868–874. [PubMed: 27627185]
70. Kashiwagi K, Yokoyama T, Nishimoto M, Takahashi M, Sakamoto A, Yonemochi M, Shirouzu M, and Ito T (2019). Structural basis for eIF2B inhibition in integrated stress response. Science 364, 495–499. [PubMed: 31048492]
71. Schoof M, Wang L, Cogan JZ, Lawrence RE, Boone M, Wuerth JD, Frost A, and Walter P (2021). Viral evasion of the integrated stress response through antagonism of eIF2-P binding to eIF2B. Nat. Commun 12, 7103. [PubMed: 34876554]
72. Wortham NC, Martinez M, Gordiyenko Y, Robinson CV, and Proud CG (2014). Analysis of the subunit organization of the eIF2B complex reveals new insights into its structure and regulation. Faseb. J 28, 2225–2237. [PubMed: 24532666]
73. Costa-Mattioli M, and Walter P (2020). The integrated stress response: From mechanism to disease. Science 368, eaat5314. [PubMed: 32327570]
74. Dever TE, Ivanov IP, and Sachs MS (2020). Conserved Upstream Open Reading Frame Nascent Peptides That Control Translation. Annu. Rev. Genet 54, 237–264. [PubMed: 32870728]
75. Pakos-Zebrucka K, Koryga I, Mnich K, Ljujic M, Samali A, and Gorman AM (2016). The integrated stress response. EMBO Rep. 17, 1374–1395. [PubMed: 27629041]
76. Costa-Mattioli M, Gobert D, Stern E, Gamache K, Colina R, Cuello C, Sossin W, Kaufman R, Pelletier J, Rosenblum K, et al. (2007). eIF2alpha phosphorylation bidirectionally regulates the switch from short- to long-term synaptic plasticity and memory. Cell 129, 195–206. [PubMed: 17418795]
77. Jiang Z, Belforte JE, Lu Y, Yabe Y, Pickel J, Smith CB, Je HS, Lu B, and Nakazawa K (2010). eIF2alpha Phosphorylation-dependent translation in CA1 pyramidal cells impairs hippocampal memory consolidation without affecting general translation. J. Neurosci 30, 2582–2594. [PubMed: 20164343]
78. Sharma V, Sood R, Khlaifia A, Eslamizade MJ, Hung TY, Lou D, Asgarihafshejani A, Lalzar M, Kiniry SJ, Stokes MP, et al. (2020). eIF2alpha controls memory consolidation via excitatory and somatostatin neurons. Nature 586, 412–416. [PubMed: 33029011]
79. Shrestha P, Ayata P, Herrero-Vidal P, Longo F, Gastone A, LeDoux JE, Heintz N, and Klann E (2020). Cell-type-specific drug-inducible protein synthesis inhibition demonstrates that memory consolidation requires rapid neuronal translation. Nat. Neurosci 23, 281–292. [PubMed: 31959934]
80. Batista G, Johnson JL, Dominguez E, Costa-Mattioli M, and Pena JL (2016). Translational control of auditory imprinting and structural plasticity by eIF2alpha. Elife 5, e17197. [PubMed: 28009255]

81. Zhang Y, Chen K, Sloan SA, Bennett ML, Scholze AR, O'Keeffe S, Phatnani HP, Guarnieri P, Caneda C, Ruderisch N, et al. (2014). An RNA-sequencing transcriptome and splicing database of glia, neurons, and vascular cells of the cerebral cortex. J. Neurosci 34, 11929–11947. [PubMed: 25186741]
82. Melas PA, Qvist JS, Deidda M, Upreti C, Wei YB, Sanna F, Fratta W, Scherma M, Fadda P, Kandel DB, and Kandel ER (2018). Cannabinoid Modulation of Eukaryotic Initiation Factors (eIF2alpha and eIF2B1) and Behavioral Cross-Sensitization to Cocaine in Adolescent Rats. Cell Rep. 22, 2909–2923. [PubMed: 29539420]
83. Kandel ER, Dudai Y, and Mayford MR (2014). The molecular and systems biology of memory. Cell 157, 163–186. [PubMed: 24679534]
84. Glock C, Biever A, Tushev G, Nassim-Assir B, Kao A, Bartnik I, Tom Dieck S, and Schuman EM (2021). The translatome of neuronal cell bodies, dendrites, and axons. Proc. Natl. Acad. Sci. USA 118. e2113929118. [PubMed: 34670838]
85. Liu J, Pasini S, Shelanski ML, and Greene LA (2014). Activating transcription factor 4 (ATF4) modulates post-synaptic development and dendritic spine morphology. Front. Cell. Neurosci 8, 177. [PubMed: 25071442]
86. Heiman M, Kulicke R, Fenster RJ, Greengard P, and Heintz N (2014). Cell type-specific mRNA purification by translating ribosome affinity purification (TRAP). Nat. Protoc 9, 1282–1291. [PubMed: 24810037]
87. tom Dieck S, Kochen L, Hanus C, Heumüller M, Bartnik I, Nassim-Assir B, Merk K, Mosler T, Garg S, Bunse S, et al. (2015). Direct visualization of newly synthesized target proteins in situ. Nat. Methods 12, 411–414. [PubMed: 25775042]
88. Schmidt EK, Clavarino G, Ceppi M, and Pierre P (2009). SUnSET, a nonradioactive method to monitor protein synthesis. Nat. Methods 6, 275–277. [PubMed: 19305406]
89. Chambers JE, Dalton LE, Clarke HJ, Malzer E, Dominicus CS, Patel V, Moorhead G, Ron D, and Marciniak SJ (2015). Actin dynamics tune the integrated stress response by regulating eukaryotic initiation factor 2alpha dephosphorylation. Elife 4, e04872. [PubMed: 25774599]
90. Chen R, Rato C, Yan Y, Crespillo-Casado A, Clarke HJ, Harding HP, Marciniak SJ, Read RJ, and Ron D (2015). G-actin provides substrate-specificity to eukaryotic initiation factor 2alpha holophosphatases. Elife 4, e04871. [PubMed: 25774600]
91. Bernstein BW, and Bamburg JR (2010). ADF/cofilin: a functional node in cell biology. Trends Cell Biol. 20, 187–195. [PubMed: 20133134]
92. Ayscough K. (1998). Use of latrunculin-A, an actin monomer-binding drug. Methods Enzymol. 298, 18–25. [PubMed: 9751867]
93. Ayscough KR (2000). Endocytosis and the development of cell polarity in yeast require a dynamic F-actin cytoskeleton. Curr. Biol 10, 1587–1590. [PubMed: 11137010]
94. Morton WM, Ayscough KR, and McLaughlin PJ (2000). Latrunculin alters the actin-monomer subunit interface to prevent polymerization. Nat. Cell Biol 2, 376–378. [PubMed: 10854330]
95. Havekes R, Park AJ, Tudor JC, Luczak VG, Hansen RT, Ferri SL, Bruinenberg VM, Poplawski SG, Day JP, Aton SJ, et al. (2016). Sleep deprivation causes memory deficits by negatively impacting neuronal connectivity in hippocampal area CA1. Elife 5, e13424. [PubMed: 27549340]
96. Choy MS, Yusoff P, Lee IC, Newton JC, Goh CW, Page R, Shenolikar S, and Peti W (2015). Structural and Functional Analysis of the GADD34:PP1 eIF2alpha Phosphatase. Cell Rep. 11, 1885–1891. [PubMed: 26095357]
97. Costa-Mattioli M, Gobert D, Harding H, Herdy B, Azzi M, Bruno M, Bidinosti M, Ben Mamou C, Marcinkiewicz E, Yoshida M, et al. (2005). Translational control of hippocampal synaptic plasticity and memory by the eIF2alpha kinase GCN2. Nature 436, 1166–1173. [PubMed: 16121183]
98. Sharma V, Ounallah-Saad H, Chakraborty D, Hleihil M, Sood R, Barrera I, Edry E, Kolatt Chandran S, Ben Tabou de Leon S, Kaphzan H, and Rosenblum K (2018). Local Inhibition of PERK Enhances Memory and Reverses Age-Related Deterioration of Cognitive and Neuronal Properties. J. Neurosci 38, 648–658. [PubMed: 29196323]
99. Zhu PJ, Huang W, Kalikulov D, Yoo JW, Placzek AN, Stoica L, Zhou H, Bell JC, Friedlander MJ, Krnjević K, et al. (2011). Suppression of PKR promotes network excitability and

enhanced cognition by interferon-gamma-mediated disinhibition. Cell 147, 1384–1396. [PubMed: 22153080]

100. Zimmermann HR, Yang W, Beckelman BC, Kasica NP, Zhou X, Galli LD, Ryazanov AG, and Ma T (2018). Genetic removal of eIF2alpha kinase PERK in mice enables hippocampal L-LTP independent of mTORC1 activity. J. Neurochem 146, 133–144. [PubMed: 29337352]
101. Ounallah-Saad H, Sharma V, Edry E, and Rosenblum K (2014). Genetic or pharmacological reduction of PERK enhances cortical-dependent taste learning. J. Neurosci 34, 14624–14632. [PubMed: 25355215]
102. Stern E, Chinnakkaruppan A, David O, Sonenberg N, and Rosenblum K (2013). Blocking the eIF2alpha kinase (PKR) enhances positive and negative forms of cortex-dependent taste memory. J. Neurosci 33, 2517–2525. [PubMed: 23392680]
103. Brush MH, and Shenolikar S (2008). Control of cellular GADD34 levels by the 26S proteasome. Mol. Cell Biol 28, 6989–7000. [PubMed: 18794359]
104. Reid DW, Tay ASL, Sundaram JR, Lee ICJ, Chen Q, George SE, Nicchitta CV, and Shenolikar S (2016). Complementary Roles of GADD34- and CReP-Containing Eukaryotic Initiation Factor 2alpha Phosphatases during the Unfolded Protein Response. Mol. Cell Biol 36, 1868–1880. [PubMed: 27161320]
105. Helseth AR, Hernandez-Martinez R, Hall VL, Oliver ML, Turner BD, Caffall ZF, Rittiner JE, Shipman MK, King CS, Gradinaru V, et al. (2021). Cholinergic neurons constitutively engage the ISR for dopamine modulation and skill learning in mice. Science 372, eabe1931. [PubMed: 33888613]
106. Manadas B, Santos AR, Szabadfi K, Gomes JR, Garbis SD, Fountoulakis M, and Duarte CB (2009). BDNF-induced changes in the expression of the translation machinery in hippocampal neurons: protein levels and dendritic mRNA. J. Proteome Res 8, 4536–4552. [PubMed: 19702335]
107. Chen PB, Kawaguchi R, Blum C, Achiro JM, Coppola G, O'Dell TJ, and Martin KC (2017). Mapping Gene Expression in Excitatory Neurons during Hippocampal Late-Phase Long-Term Potentiation. Front. Mol. Neurosci 10, 39. [PubMed: 28275336]
108. Ma Y, and Hendershot LM (2003). Delineation of a negative feedback regulatory loop that controls protein translation during endoplasmic reticulum stress. J. Biol. Chem 278, 34864–34873. [PubMed: 12840028]
109. Novoa I, Zeng H, Harding HP, and Ron D (2001). Feedback inhibition of the unfolded protein response by GADD34-mediated dephosphorylation of eIF2alpha. J. Cell Biol 153, 1011–1022. [PubMed: 11381086]
110. Young SK, Willy JA, Wu C, Sachs MS, and Wek RC (2015). Ribosome Reinitiation Directs Gene-specific Translation and Regulates the Integrated Stress Response. J. Biol. Chem 290, 28257–28271. [PubMed: 26446796]
111. Lee YY, Cevallos RC, and Jan E (2009). An upstream open reading frame regulates translation of GADD34 during cellular stresses that induce eIF2alpha phosphorylation. J. Biol. Chem 284, 6661–6673. [PubMed: 19131336]
112. Doerfel LK, Wohlgemuth I, Kothe C, Peske F, Urlaub H, and Rodnina MV (2013). EF-P is essential for rapid synthesis of proteins containing consecutive proline residues. Science 339, 85–88. [PubMed: 23239624]
113. Gutierrez-Uzquiza A, Colon-Gonzalez F, Leonard TA, Canagarajah BJ, Wang H, Mayer BJ, Hurley JH, and Kazanietz MG (2013). Coordinated activation of the Rac-GAP beta2-chimaerin by an atypical proline-rich domain and diacylglycerol. Nat. Commun 4, 1849. [PubMed: 23673634]
114. Melnikov S, Mailliot J, Rigger L, Neuner S, Shin BS, Yusupova G, Dever TE, Micura R, and Yusupov M (2016). Molecular insights into protein synthesis with proline residues. EMBO Rep. 17, 1776–1784. [PubMed: 27827794]
115. Ude S, Lassak J, Starosta AL, Kraxenberger T, Wilson DN, and Jung K (2013). Translation elongation factor EF-P alleviates ribosome stalling at polyproline stretches. Science 339, 82–85. [PubMed: 23239623]

116. Kozak M. (2001). Constraints on reinitiation of translation in mammals. Nucleic Acids Res. 29, 5226–5232. [PubMed: 11812856]
117. Luukkonen BG, Tan W, and Schwartz S (1995). Efficiency of reinitiation of translation on human immunodeficiency virus type 1 mRNAs is determined by the length of the upstream open reading frame and by intercistronic distance. J. Virol 69, 4086–4094. [PubMed: 7769666]
118. Rajkowitsch L, Vilela C, Berthelot K, Ramirez CV, and McCarthy JEG (2004). Reinitiation and recycling are distinct processes occurring downstream of translation termination in yeast. J. Mol. Biol 335, 71–85. [PubMed: 14659741]
119. Broix L, Turchetto S, and Nguyen L (2021). Coordination between Transport and Local Translation in Neurons. Trends Cell Biol. 31, 372–386. [PubMed: 33526339]
120. Briz V, Zhu G, Wang Y, Liu Y, Avetisyan M, Bi X, and Baudry M (2015). Activity-dependent rapid local RhoA synthesis is required for hippocampal synaptic plasticity. J. Neurosci 35, 2269–2282. [PubMed: 25653381]
121. Chen LY, Rex CS, Casale MS, Gall CM, and Lynch G (2007). Changes in synaptic morphology accompany actin signaling during LTP. J. Neurosci 27, 5363–5372. [PubMed: 17507558]
122. Zhou Q, Homma KJ, and Poo MM (2004). Shrinkage of dendritic spines associated with long-term depression of hippocampal synapses. Neuron 44, 749–757. [PubMed: 15572107]
123. Bosch M, Castro J, Saneyoshi T, Matsuno H, Sur M, and Hayashi Y (2014). Structural and molecular remodeling of dendritic spine substructures during long-term potentiation. Neuron 82, 444–459. [PubMed: 24742465]
124. Jędrzejewska-Szmek J, and Blackwell KT (2019). From membrane receptors to protein synthesis and actin cytoskeleton: Mechanisms underlying long lasting forms of synaptic plasticity. Semin. Cell Dev. Biol 95, 120–129. [PubMed: 30634048]
125. Yuen EY, Liu W, Kafri T, van Praag H, and Yan Z (2010). Regulation of AMPA receptor channels and synaptic plasticity by cofilin phosphatase Slingshot in cortical neurons. J. Physiol 588, 2361–2371. [PubMed: 20442266]
126. Zhou L, Jones EV, and Murai KK (2012). EphA signaling promotes actin-based dendritic spine remodeling through slingshot phosphatase. J. Biol. Chem 287, 9346–9359. [PubMed: 22282498]
127. Gu J, Lee CW, Fan Y, Komlos D, Tang X, Sun C, Yu K, Hartzell HC, Chen G, Bamburg JR, and Zheng JQ (2010). ADF/cofilin-mediated actin dynamics regulate AMPA receptor trafficking during synaptic plasticity. Nat. Neurosci 13, 1208–1215. [PubMed: 20835250]
128. De Rubeis S, Pasciuto E, Li KW, Fernández E, Di Marino D, Buzzi A, Ostroff LE, Klann E, Zwartkruis FJT, Komiyama NH, et al. (2013). CYFIP1 coordinates mRNA translation and cytoskeleton remodeling to ensure proper dendritic spine formation. Neuron 79, 1169–1182. [PubMed: 24050404]
129. Santini E, Huynh TN, Longo F, Koo SY, Mojica E, D'Andrea L, Bagni C, and Klann E (2017). Reducing eIF4E-eIF4G interactions restores the balance between protein synthesis and actin dynamics in fragile X syndrome model mice. Sci. Signal 10, eaan0665. [PubMed: 29114037]
130. Nectow AR, Moya MV, Ekstrand MI, Mousa A, McGuire KL, Sferrazza CE, Field BC, Rabinowitz GS, Sawicka K, Liang Y, et al. (2017). Rapid Molecular Profiling of Defined Cell Types Using Viral TRAP. Cell Rep. 19, 655–667. [PubMed: 28423326]
131. Schneider CA, Rasband WS, and Eliceiri KW (2012). NIH Image to ImageJ: 25 years of image analysis. Nat. Methods 9, 671–675. [PubMed: 22930834]
132. Martin M. (2011). Cutadapt removes adapter sequences from high-throughput sequencing reads. EMBnet. j 17, 10–12.
133. Zhang Y, Parmigiani G, and Johnson WE (2020). ComBat-seq: batch effect adjustment for RNA-seq count data. NAR Genom. Bioinform 2, lqaa078. [PubMed: 33015620]
134. Love MI, Huber W, and Anders S (2014). Moderated estimation of fold change and dispersion for RNA-seq data with DESeq2. Genome Biol. 15, 550. [PubMed: 25516281]
135. Kolde R. (2019). Pheatmap: Pretty Heatmaps. R Package. version 1.0.12 https://CRAN.R-project.org/package=pheatmap.
136. Yu G, Wang LG, Han Y, and He QY (2012). clusterProfiler: an R package for comparing biological themes among gene clusters. OMICS 16, 284–287. [PubMed: 22455463]

137. Dobin A, Davis CA, Schlesinger F, Drenkow J, Zaleski C, Jha S, Batut P, Chaisson M, and Gingeras TR (2013). STAR: ultrafast universal RNA-seq aligner. Bioinformatics 29, 15–21. [PubMed: 23104886]

138. Zhu A, Ibrahim JG, and Love MI (2019). Heavy-tailed prior distributions for sequence count data: removing the noise and preserving large differences. Bioinformatics 35, 2084–2092. [PubMed: 30395178]

139. Aryal S, Longo F, and Klann E (2021). Genetic removal of p70 S6K1 corrects coding sequence length-dependent alterations in mRNA translation in fragile X syndrome mice. Proc. Natl. Acad. Sci. USA 118. e2001681118. [PubMed: 33906942]

140. Koopmans F, van Nierop P, Andres-Alonso M, Byrnes A, Cijsouw T, Coba MP, Cornelisse LN, Farrell RJ, Goldschmidt HL, Howrigan DP, et al. (2019). SynGO: An Evidence-Based, Expert-Curated Knowledge Base for the Synapse. Neuron 103, 217–234.e4. [PubMed: 31171447]

Highlights

- GADD34 is translated by neurons in response to neuronal activation
- GADD34 promotes fast dephosphorylation of eIF2α and elevation of neuronal protein synthesis
- GADD34-eIF2α interaction requires actin monomers and cofilin activity
- Artificially increasing cofilin activity in neurons promotes *de novo* protein synthesis

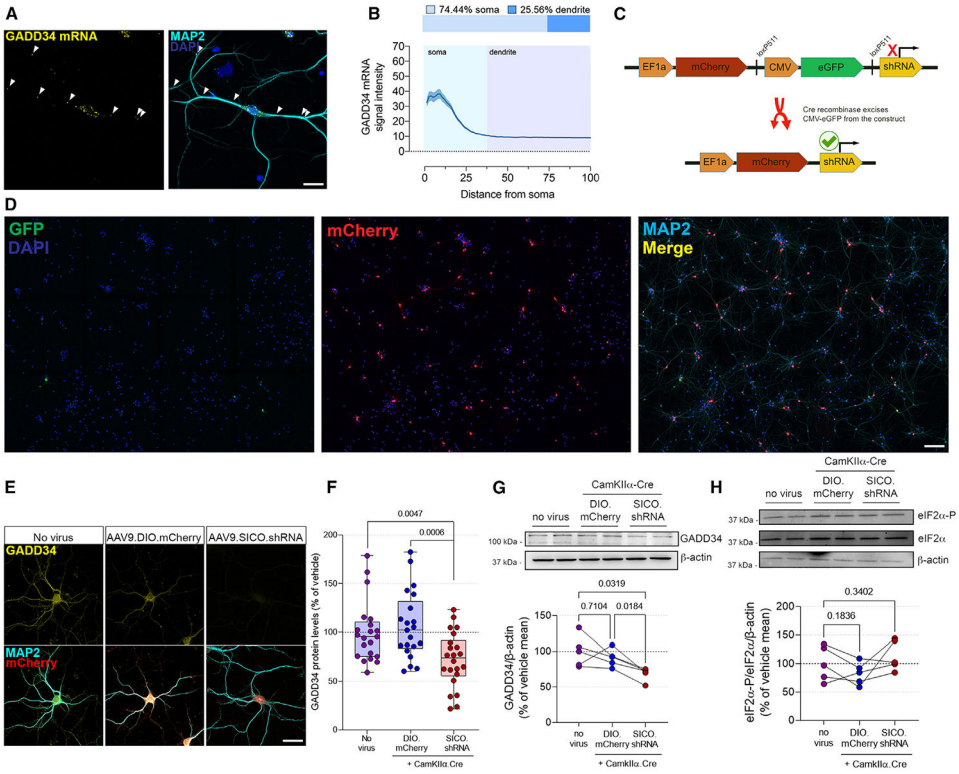

Figure 1. GADD34 is constitutively expressed in neurons

(A) Fluorescence *in situ* hybridization (FISH) targeting GADD34 mRNA (punctate signal). Green, FISH; blue, DAPI; cyan, MAP2. Scale bar: 50 μm.

(B) Top: percentage of total mRNA localized to somatic vs. dendritic compartments. Bottom: radial quantification of GADD34 mRNA puncta in neurons, from soma (light blue background) to dendritic portions (dark blue background) (n = 34 neurons/3 independent cultures).

(C) SICO.shRNA system for knockdown of GADD34.

(D) Neurons transduced with AAV9.EF1α.mCherry.SICO-shRNA.*Ppp1r15a*. Scale bar: 200 μm.

(E) Representative images of GADD34 immunostaining in neurons transduced with AAV9.EF1α.mCherry.SICO-shRNA.*Ppp1r15a*. Yellow, GADD34; cyan, MAP2; red, mCherry. Scale bar: 50 μm.

(F) Quantification of (E) (n = 20–23 neurons from 2 independent cultures). One-way ANOVA followed by Dunnett post hoc test. Error bars represent min to max values.

(G) Western blot of cell lysates obtained from naive neurons or co-transduced with AAV9.CamKIIα.Cre + AAV9.hSyn2.DIO.mCherry or AAV9.CamKIIα.Cre + AAV9.EF1α.mCherry.SICO-shRNA.*Ppp1r15a* (n = 5 independent cultures). Top row, GADD34; bottom row, β-actin. One-way ANOVA followed by Dunnet post hoc test.

(H) Western blot of cell lysates obtained from naive neurons or co-transduced with AAV9.CamKIIα.Cre + AAV9.hSyn2.DIO.mCherry or AAV9.CamKIIα.Cre + AAV9.EF1α.mCherry.SICO-shRNA.*Ppp1r15a* (n = 5 independent cultures). Top row, eIF2α-P; middle row, total eIF2α; bottom row, β-actin. One-way ANOVA followed by Dunnet post hoc test.

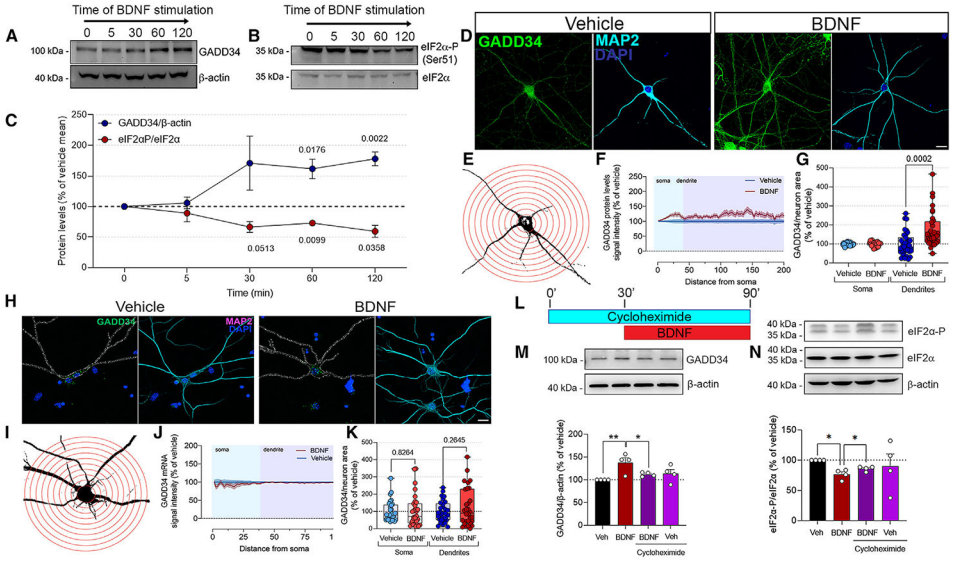

Figure 2. BDNF promotes transcription-independent increase in GADD34 protein levels

(A) Western blot probed for GADD34 (top blot) or β-actin control (bottom lane) using samples obtained from neurons exposed to BDNF at time points indicated.

(B) Western blot probed for eIF2α-P (Ser51, top lane) or total eIF2α (bottom lane) using the same samples described in (A).

(C) Quantification of (A) and (B) (n = 5 independent primary cultures). One-way ANOVA repeated measures followed by Dunnett post hoc test.

(D) Immunofluorescence staining for GADD34 in neurons. Green, GADD34; cyan, MAP2; blue, DAPI. Scale bar: 50 μm.

(E) Representation of the radial quantification of GADD34 expression in neurons.

(F) Radial quantification of GADD34 expression in soma (light blue background) and in dendrites (dark blue background) of neurons exposed to either vehicle (blue line) or BDNF for 1 h (red line). Light shade surrounding the lines represents SEM.

(G) Total amount of GADD34 in either soma or dendrites of neurons exposed to either vehicle or 50 ng/mL BDNF for 1 h. Statistical analysis was performed to compare differences in each compartment, independently (n = 37–38 neurons/condition from 3 independent cultures). Unpaired t test. Error bars represent min to max values. See STAR Methods for details on the quantification.

(H) RNA-scope-based FISH staining against GADD34 mRNA in neurons. Green, FISH; cyan, MAP2; blue, DAPI. Scale bar: 50 μm.

(I) Representation of the radial quantification of *Ppp1r15a* mRNA expression in primary neurons.

(J) Radial quantification of *Ppp1r15a* mRNA expression in soma (light blue background) and in dendrites (dark blue background) of neurons exposed to either vehicle (blue line) or BDNF (red line) for 1 h. Light shade surrounding the lines represent SEM.

(K) Total amounts of *Ppp1r15a* mRNA in either soma or dendrites of neurons exposed to either vehicle or BDNF for 1 h (n = 33–34 neurons/condition from 3 independent cultures). Error bars represent min to max values. See STAR Methods.

(L) Representation of timeline for experiment with cycloheximide and BDNF.

(M) Western blot using samples obtained from neurons treated as described in (L) (n = 4 independent cultures). Top row, GADD34; bottom row = β-actin. Two-way ANOVA followed by Tukey's post hoc test, $p_{(Veh\ vs.\ BDNF)} = 0.0357$; $p_{(BDNF\ vs.\ BDNF+Chx)} = 0.0029$. Mean ± SEM.

(N) Western blot using samples obtained from neurons treated as described in (L) (n = 4 independent cultures). Top row, eIF2α-P; middle row, total eIF2α; bottom row, β-actin. Two-way ANOVA followed by Tukey's post hoc test, $p_{(Veh\ vs.\ BDNF)} = 0.0111$; $p_{(BDNF\ vs.\ BDNF+Chx)} = 0.0231$. Mean ± SEM.

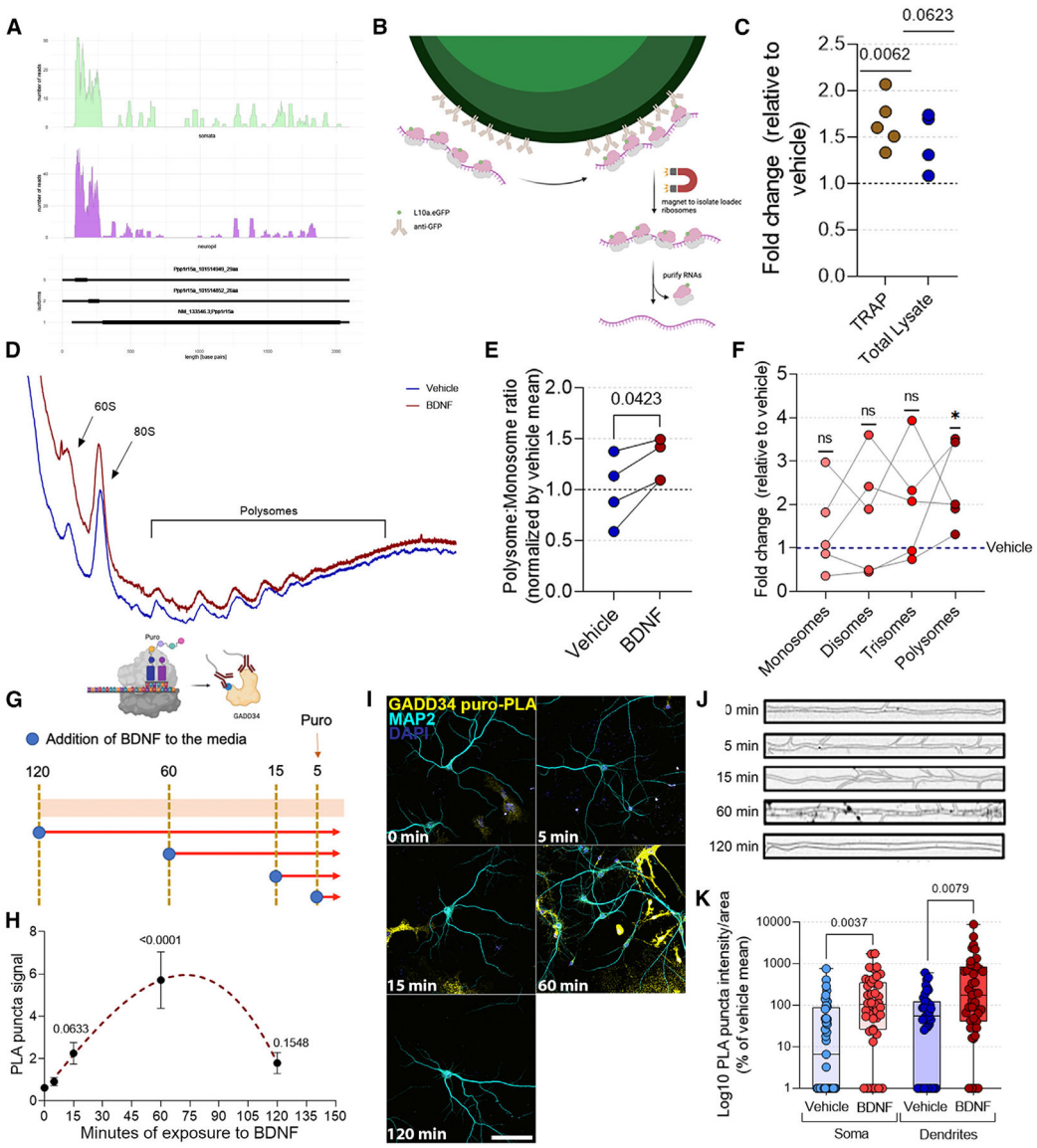

Figure 3. BDNF increases GADD34 translation in neurons

(A) Ribo-seq data from Glock et al.[24] indicating stalled ribosomes at the uORFs of *Ppp1r15a* mRNA in neuronal soma and dendrites.

(B) Schematics of the workflow for TRAP-qPCR. See STAR Methods.

(C) TRAP-qPCR and qPCR (total lysate) analysis of *Ppp1r15a* normalized by *Gapdh* (n = 4–5 independent cultures). Wilcoxon rank test.

(D) Representative polysome fractionation from neurons exposed to either vehicle (red) or BDNF for 1 h (blue).

(E) Polysome/monosome ratio. Paired t test, p = 0.0411. Unpaired t test, p = 0.2094.

(F) Quantification of loaded *Ppp1r15a* mRNA in different fractions of polysome profiling, assessed by real-time PCR (n = 5 independent primary cultures). Blue dashed line represents vehicle, normalized to 1 in every fraction. Statistical analyses were performed comparing the mean variations per fraction. Wilcoxon rank test, ns, non-significant, p = 0.0314.

(G) Puro-PLA experimental design.

(H) Quantification of total puro-PLA signal in neurons exposed to BDNF in time points indicated (n = 35–36 neurons from 3 independent cultures). One-way ANOVA repeated measures followed by Dunnett post hoc test.
(I) Representative images of puro-PLA from the experiment described in (H). Green, puro-PLA; red, MAP2; blue, DAPI. Scale bar: 150 μm.
(J) Representative images of dendritic signal from the puro-PLA time course experiment. PLA signals are represented as black dots.
(K) Quantification of GADD34 puro-PLA signal at the 60 min time point of exposure to BDNF, isolating somatic and dendritic compartments (n = 35–36 neurons from 3 independent cultures). Unpaired t test. Error bars represent min to max values. See STAR Methods.

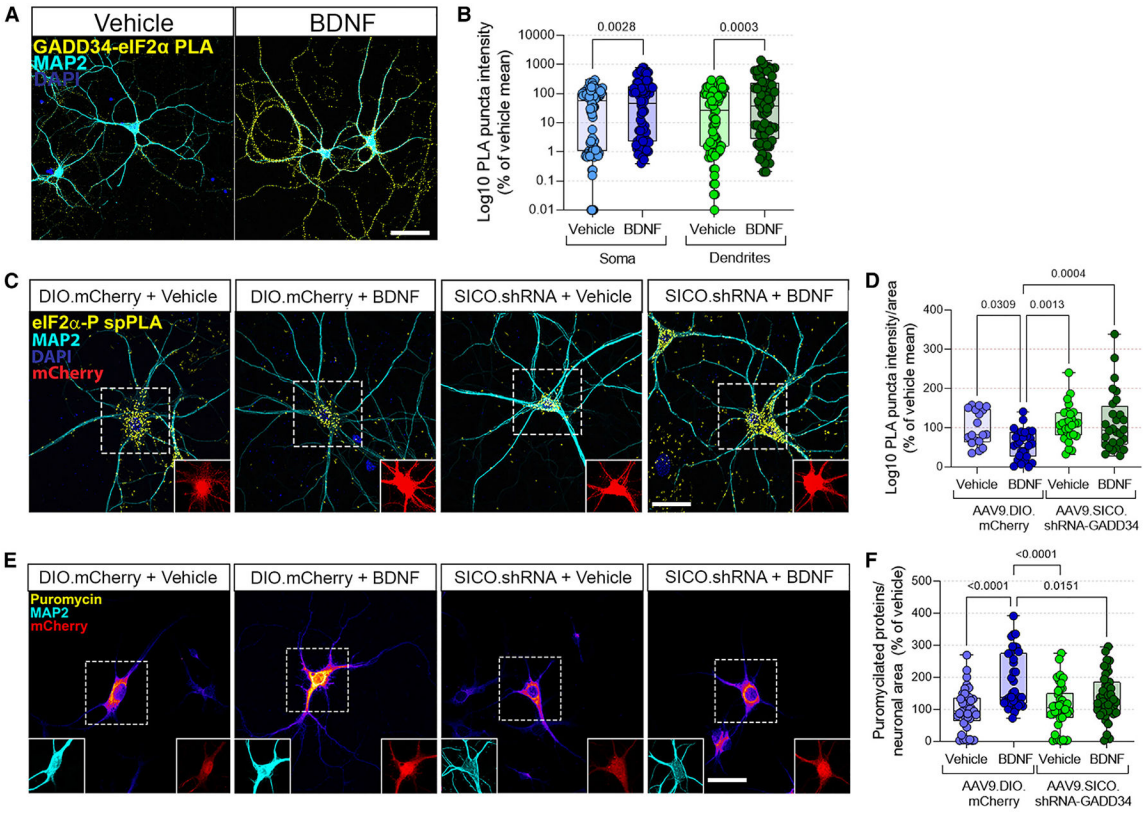

Figure 4. BDNF promotes GADD34-eIF2α interactions and GADD34-dependent protein synthesis

(A) Representative images of GADD34-eIF2α PLA in neurons. Green, PLA; red, MAP2; blue, DAPI. Scale bar: 100 μm.

(B) Quantification of (D) (N = 50 neurons from 3 independent cultures). Statistical analysis was performed comparing each compartment independently. Unpaired t test. Error bars represent min to max values. See STAR Methods.

(C) Representative images of eIF2α-P levels measured using spPLA in neurons transduced with either AAV9.EF1α.mCherry.SICO-shRNA.*Ppp1r15a* or control AAV9.hSyn.DIO.mCherry. Cyan, MAP2; red, mCherry; yellow, eIF2α-P. Scale bar: 50 μm.

(D) Quantification of (F) (n = 18–29 neurons/condition from 3 independent cultures). Two-way ANOVA followed by Tukey's post hoc test. Error bars represent min to max values.

(E) Representative images of *de novo* protein synthesis measured using *in situ* SUnSET in neurons transduced with either AAV9.EF1α.mCherry.SICO-shRNA.*Ppp1r15a* or control AAV9.hSyn.DIO.mCherry. Cyan, MAP2; red, mCherry; pseudo color, puromycin. Scale bar: 50 μm.

(F) Quantification of (F) (n = 28–41 neurons/condition from 3 independent cultures). Two-way ANOVA followed by Tukey's post hoc test. Error bars represent min to max values.

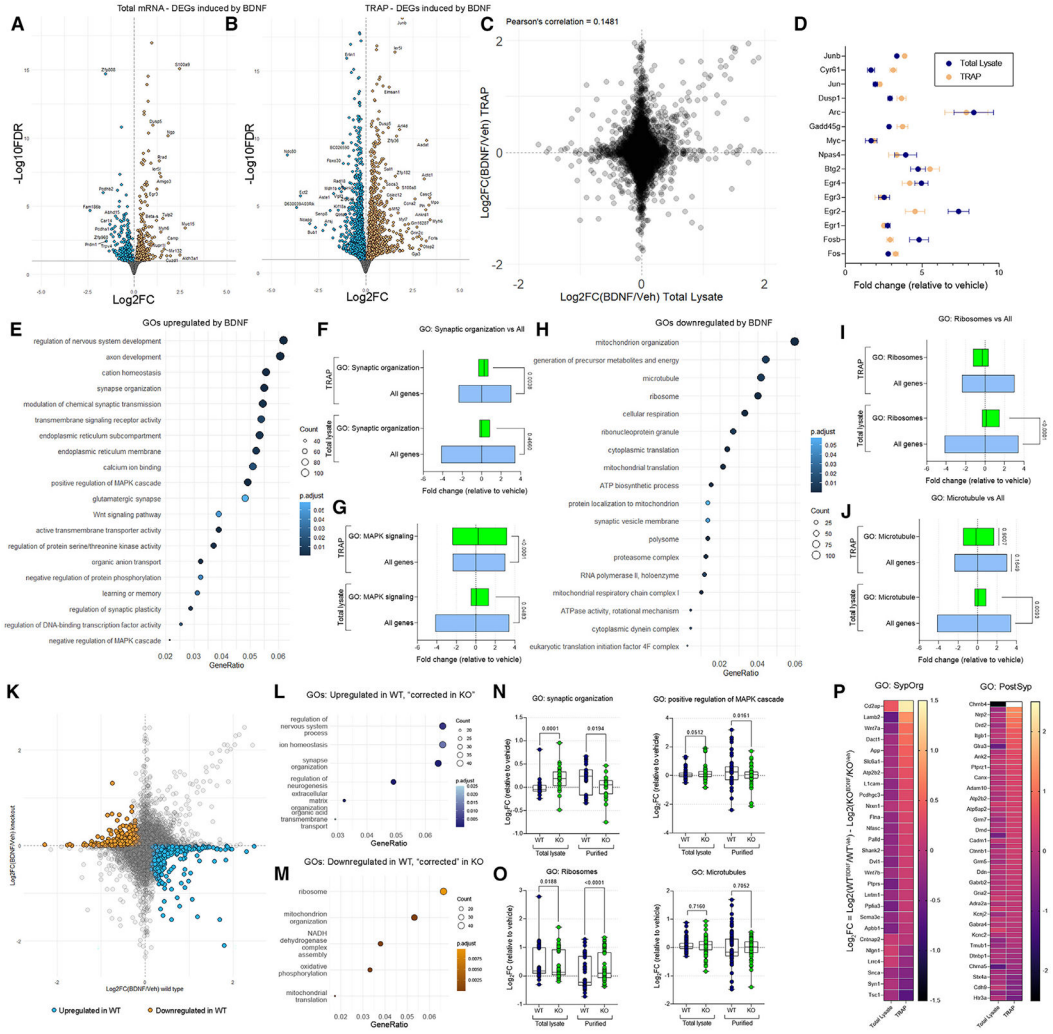

Figure 5. GADD34 mediates the BDNF-induced translation of mRNAs that encode synaptic-plasticity-related proteins

(A) Volcano plot demonstrating $\log_2$FC of upregulated (orange) and downregulated (blue) mRNAs in total mRNA fraction.

(B) Volcano plot demonstrating $\log_2$FC of upregulated (orange) and downregulated (blue) mRNAs in the TRAP purified fraction.

(C) Correlation plot between $\log_2$FCs of total mRNA fraction (x axis) vs. TRAP fraction (y axis). Each black dot is an individual mRNA.

(D) FCs of IEGs induced by BDNF both in total fraction (blue) and TRAP fraction (beige).

(E) GO analysis of DEGs significantly upregulated by BDNF. Size of circle indicates counts of mRNAs in each group, and color indicates adjusted p value of that GO group.

(F) Comparison of $\log_2$FCs of mRNAs belonging to the "synapse organization" GO and all mRNAs identified in total mRNA or TRAP fractions. Gene ratio, the number of genes identified in each group divided by the amount of background genes. Unpaired t test.

(G) Comparison of $\log_2$FCs of mRNAs belonging to the "positive regulation of MAPK cascade" GO and all mRNAs identified in total mRNA or TRAP fractions. Gene ratio is the same as in (F). Unpaired t test.

(H) GO analysis of DEGs significantly downregulated by BDNF. Size of circle indicates counts of mRNAs in each group, and color indicates adjusted p value of that GO group.
(I) Comparison of log_2FCs of mRNAs belonging to the “ribosome” GO and all mRNAs identified in total mRNA or TRAP fractions. Gene ratio is the same as in (F). Unpaired t test.
(J) Comparison of log_2FCs of mRNAs belonging to the “microtubule” GO and all mRNAs identified in total mRNA or TRAP fractions. Gene ratio is the same as in (F). Unpaired t test.
(K) Correlation plot between log_2FCs of WT (x axis) vs. KO cells (y axis). Each dot is an individual mRNA. Orange dots indicate mRNAs that are downregulated in WT, corrected in KO. Blue dots indicate mRNAs that are upregulated in WT, corrected in KO.
(L) GO analysis of DEGs significantly upregulated by BDNF, corrected in KO. Size of circle indicates counts of mRNAs in each group, and color indicates adjusted p value of that GO group.
(M) GO analysis of DEGs significantly downregulated by BDNF, corrected in KO. Size of circle indicates the total count of mRNAs in each group, and color indicates adjusted p value of that GO group.
(N) Comparison of log_2FC WT vs. log_2FC KO of mRNAs belonging to the “synaptic organization” or “positive regulation of MAPK cascade” GOs. Comparisons were made in total and TRAP fractions. Unpaired t test.
(O) Comparison of log_2FC WT vs. log_2FC KO of mRNAs belonging to the “ribosome” or “microtubule” GOs. Comparisons were made in total and TRAP fractions. Unpaired t test.
(P) Heatmaps comparing the log_2FCs of mRNAs belonging to either “synaptic organization” or “post-synapse.” Comparisons were performed in total and TRAP fractions.

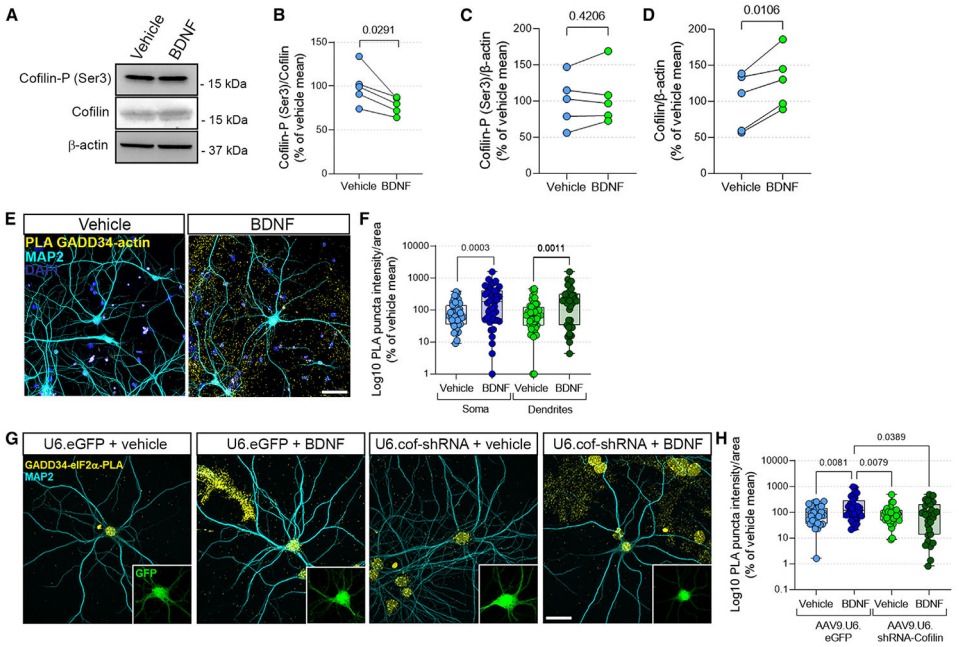

Figure 6. BDNF increases the physical interaction between G-actin and GADD34

(A) Representative western blots probed cofilin-P (ser 3, top row), total cofilin (middle row), and β-actin (bottom row) using samples from neurons exposed to vehicle or BDNF for 1 h.

(B) Quantification of the ratio of cofilin-P over cofilin (n = 3 primary cultures). Paired t test. Unpaired t test, p = 0.0743.

(C) Quantification of the ratio of cofilin-P over β-actin (n = 3 primary cultures). Paired t test. Unpaired t test, p = 0.8249.

(D) Quantification of the ratio of cofilin over β-actin (n = 3 primary cultures). Paired t test. Unpaired t test, p = 0.2710.

(E) Representative images of the PLA for GADD34-pan actin in primary neurons. Insets represent the PLA signal in the soma (black dots). Below the images are dendritic representations of the PLA signal. Yellow, PLA GADD34-eIF2α; cyan, MAP2; blue, DAPI. Scale bar: 100 μm.

(F) Quantification of (G) (n = 39–44 neurons from 3 independent cultures). Statistical analysis was performed to compare differences in each compartment, independently. Unpaired t test. Error bars represent min to max values. See STAR Methods.

(G) Representative images of GADD34-eIF2α PLA in primary neurons transduced with AAV9.U6.shRNA-cofilin or control and then exposed to BDNF for 1 h. Yellow, GADD34-eIF2α PLA; cyan, MAP2. Scale bar: 50 μm.

(H) Quantification of (I) (n = 29–31 neurons/group from 3 independent cultures). Two-way ANOVA followed by Dunnet's post hoc test. Error bars represent min to max values.

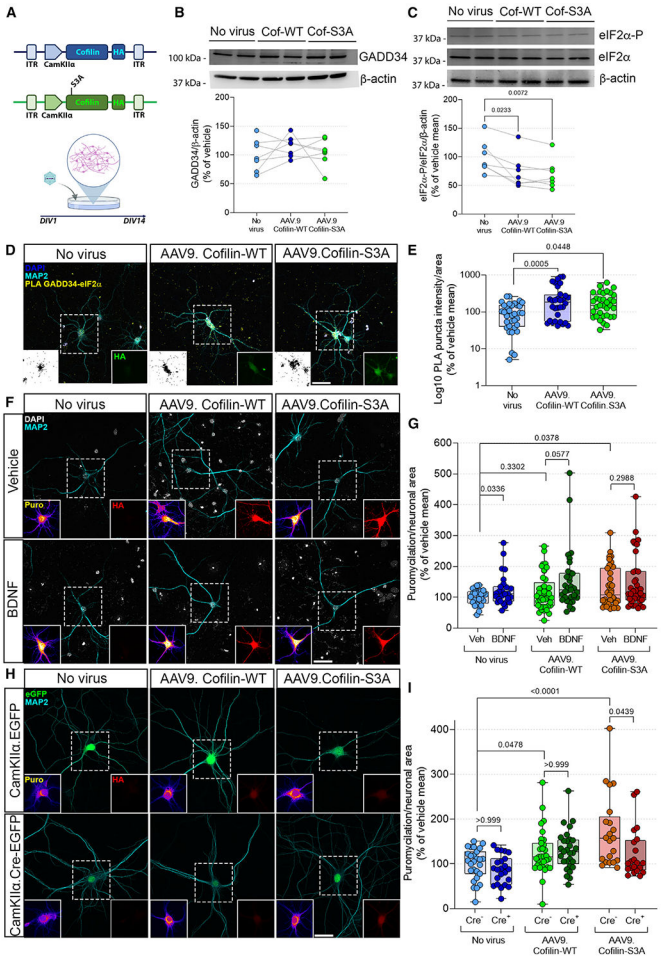

Figure 7. Increasing cofilin activity promotes protein synthesis and eIF2α dephosphorylation

(A) Viral system used to overexpress WT or mutant cofilin in primary neurons.

(B) Western blot probed for GADD34 (top lane) or β-actin (bottom lane) on samples from neurons transduced with either no virus, cof-WT, or cof-S3A. Below is the quantification of GADD34 normalized by β-actin (n = 5 independent primary cultures). One-way ANOVA followed by Dunnett post hoc test.

(C) Top: western blot probed for eIF2α-P (ser 5, top lane), total eIF2α (middle lane), or β-actin (bottom lane) on samples from neurons transduced with no virus, cof-WT, or cof-S3A. Bottom: quantification of eIF2α-P normalized by eIF2α and β-actin (n = 5 independent primary cultures). One-way ANOVA followed by Dunnett post hoc test.

(D) Representative images of GADD34-eIF2α PLA in neurons transduced with no virus, AAV5.CamKIIα.Cof-WT-HA, or AAV5.CamKIIα.Cof-S3A-HA. Yellow, PLA; cyan, MAP2; blue, DAPI; green, HA (bottom right inset). Scale bar: 100 μm.

(E) Quantification of the total PLA signal normalized by the neuronal area (n = 32–34 neurons from 3 independent cultures). One-way ANOVA followed by Dunnett post hoc test. Error bars represent min to max values.

(F) Representative images of *in situ* SUnSET in neurons transduced with no virus (left column), AAV5.CamKIIα.Cof-WT-HA (middle column), or AAV5.CamKIIα.Cof-S3A-HA (right column), exposed to vehicle (top row) or BDNF (bottom row). Cyan, MAP2; gray,

DAPI; pseudo color, puromycin (bottom left inset); red, HA (bottom right inset). Scale bar: 100 μm.

(G) Quantification of (E) (n = 27–41 neurons from 3 independent cultures). Comparisons of vehicle vs. BDNF for each group (no virus, cof-WT, or cof-S3A): unpaired t test. Comparisons between groups: one-way ANOVA followed by Dunnett's post hoc test. Error bars represent min to max values.

(H) Representative images of *in situ* SUnSET in neurons transduced with no virus (left column), AAV5.CamKIIα.Cof-WT-HA (middle column), or AAV5.CamKIIα.Cof-S3A-HA (right column), co-transduced with CamKIIα.EGFP (top row) or CamKIIα.Cre-EGFP (bottom row). Cyan, MAP2; green, EGFP; pseudo color, puromycin (bottom left inset); red, HA (bottom right inset). Scale bar: 50 μm.

(I) Quantification of (H) (n = 21–31 neurons from 3 independent cultures). Comparisons of vehicle vs. BDNF for each group (no virus, cof-WT, or cof-S3A): unpaired t test. Comparisons between groups: two-way ANOVA followed by Dunnett's post hoc test. Error bars represent min to max values.

KEY RESOURCES TABLE

REAGENT or RESOURCE	SOURCE	IDENTIFIER
Antibodies		
GFP (1:1000)	ThermoFisher	AB_2536526
mCherry (1:500)	Invitrogen	AB-2536611
MAP2 (1:2000)	Encor Biotech	AB_2138173
GADD34 (1:500)	Proteintech	AB_2168724
β-actin (1:10000)	Sigma Aldrich	AB_476697
eIF2a-P (Ser51) (1:1000)	Cell Signaling	AB_330951
eIF2a-P (Ser51) (1:1000)	Cell Signaling	AB_2096481
eIF2a (1:500)	Cell Signaling	AB_2230924
eIF2a (1:500)	Abcam	AB_304838
Puromycin (1:500)	Millipore	AB_2566826
HtzGFP-19C8 (50 mg per reaction)	Sloan Kettering	Custom
HtzGFP-19F7 (50 mg per reaction)	Sloan Kettering	Custom
Cofilin-P (Ser3) (1:2000)	Cell Signaling	AB_2080597
Cofilin (1:1000)	Cell Signaling	AB_10622000
Pan-actin (1:10000)	Novus Biological	AB_787881
HA tag (1:1000)	Cell Signaling	AB_1549585
HA tag (1:100)	Millipore	AB_390918
Goat anti-Rat 568 (1:500)	Thermo Fisher	AB_2534121
Goat anti-Chicken 647 (1:500)	Thermo Fisher	AB_2535866
Goat anti-Mouse 647 (1:500)	Thermo Fisher	AB_2535805
Goat anti-Rabbit 488 (1:500)	Thermo Fisher	AB_143165
Goat anti-Chicken 405 (1:500)	Thermo Fisher	AB_2890271
Goat anti-Rabbit HRP (1:10000)	Fisher Scientific	AB_1965959
Goat anti-Mouse HRP (1:10000)	Fisher Scientific	AB_1965958
Bacterial and virus strains		
AAV9.CamKIIα.0.4.Cre.SV40	pENN.AAV.CamKII 0.4.Cre.SV40 was a gift from James M. Wilson (Addgene viral prep # 105558-AAV9)	Addgene_105558
AAV9.hSyn.DIO.mCherry	pAAV-hSyn-DIO-mCherry was a gift from Bryan Roth (Addgene viral prep # 50459-AAV9)	Addgene_50459
AAV9.CamKIIα.HI.GFP-Cre.WPRE.SV40	pENN.AAV.CamKII.HI.GFP-Cre.WPRE.SV40 was a gift from James M. Wilson (Addgene viral prep # 105551-AAV9)	Addgene_105551
AAV9.CamKIIα0.4.eGFP.WPRE.rBG	pENN.AAV.CamKII0.4.eGFP.WPRE.rBG was a gift from James M. Wilson (Addgene viral prep # 105541-AAV9)	Addgene_105541
AAV9.EF1α.mCherry.SICO.shRNA-GADD34	Vector Biolabs	Custom
AAV9.GFP.U6.CFL1-shRNA	Vector Biolabs	shAAV-255337
AAV5.FLEX.EGFP-L10a	pAAV-FLEX-EGFPL10a was a gift from Nathaniel Heintz & Alexander Nectow & Eric Schmidt (Addgene viral prep # 98747-AAV5)[130]	(Nectow et al., 2017)[130] Addgene_98747

REAGENT or RESOURCE	SOURCE	IDENTIFIER
AAV5.CamKIIα.Cofilin-WT-HA	(Havekes et al., 2016)[95]	N/A
AAV5.CamKIIα.Cofilin-S3A-HA	(Havekes et al., 2016)[95]	N/A
Chemicals, peptides, and recombinant proteins		
Cycloheximide	Sigma Aldrich	239764
Thapsigargin	Thermo Fisher	T7458
Puromycin	Sigma Aldrich	P8833
Latrunculin A	Thermo Fisher	L12370
Tamoxifen diet	Envigo	TD130859
BDNF	Peprotech	450–02
Paraformaldehyde	EMS	15714
Tris-glycine gels (4–20% gradient)	Thermo Fisher	XP04200BOX
Transfer stacks	Thermo Fisher	IB24002
Dyanbeads MyOne Streptavidin T1	Thermo Fisher	65601
Protein L, Biotinylated	Thermo Fisher	29997
Protease and Phosphatase Inhibitor	Thermo Fisher	78441
RNAsin	Promega	N2615
SuperaseIn	Life Technologies	AM2694
RNAse-Free NP-40	AG scientific	P1505
TRIzol reagent	Thermo Fisher	15596026
RNAScope probe mm-PPP1R15A	ACD Bio	556031
Nuclease-free water	Thermo Fisher	4387936
MgCl2 (1M)	Thermo Fisher	AM9530G
HEPES (1M, pH 7.3)	Fisher Scientific	AAJ16924AE
PBS 10x (RNAse-free)	Thermo Fisher	AM9625
KCl (2M)	Thermo Fisher	AM9640G
RIPA buffer	Thermo Fisher	89901
Neurobasal Plus	Thermo Fisher	A3582901
B27 Plus supplement	Thermo Fisher	A3582801
Penicilin/Streptomycin	Fisher Scientific	15140122
GlutaMAX	Life Technologies	35050061
Coverslips	NeuVitro	GG-18-Laminin
Poly-L-ornithine 0.01%	Millipore	A-004-C
Phosphate-buffered saline	Corning	21-040-CV
DMEM + glucose	Gibco	10569010
Fetal bovine serum	Gibco	10-438-026
HBSS	Life Technologies	14025134
Laminin	Sigma Aldrich	L2020-1MG
5-Fluoro-2′-Uridine (FUDR)	Sigma Aldrich	F-0503
DTT 1M	Sigma Aldrich	646563-10x
DHPC	Avanti Polar Lipids	850306P
Critical commercial assays		
Duolink *in situ* Proximity Ligand Assay kit	Sigma Aldrich	DUO92008

REAGENT or RESOURCE	SOURCE	IDENTIFIER
NaveniFlex MR	Navinci	NAV-NF.MR.100
NaveniFlex RR	Navinci	NAV-NF.RR.100
Agilent HS TapeStation	Agilent	50675584
Quant-it	Invitrogen	P11495
Takara SMART-Seq HT kit	Takara Bio	634438
RNEasy Plus Mini Kit	Qiagen	74134
Nextera XT DNA library kit	Illumina	FC-131-1096
Direct-Zol RNA Miniprep Plus kit	Zymogen	R2070
RNAScope Fluorescent Multiplex Kit	ACD Bio	320850
Luna Universal One-Step RT-qPCR kit	New England Biolabs	E3006S
ECL kits	Cytiva	RPN2108
Deposited data		
TRAP-seq dataset	This manuscript	GSE248013 GEO Accession viewer (nih.gov)
Experimental models: Organisms/strains		
C57/Bl6J	Jackson lab	IMSR_JAX:000664
B6N.129P2(Cg)-*Ppp1r15a*$^{tm1.1Ajf}$/Mmnc (GADD34^{flfl})	MMRRC	MMRRC_030266-UNC
Oligonucleotides		
PPP1R15A_Fwd	This study	5′-TCCGACTGCAAAGGCGGCTCA-3′
PPP1R15A_Rev	This study	5′-CAGCCAGGAAATGGACAGTGAC-3′
GAPDH_Fwd	This study	5′-CATCACTGCCACCCAGAAGACTG-3′
GAPDH_Rev	This study	5′-ATGCCAGTGAGCTTCCCGTTCAG-3′
Software and algorithms		
Graphpad Prism – v9.3.1	GraphPad	SCR_002798 Company - GraphPad
ImageJ – v1.53c	(Schneider et al., 2012)[131]	SCR_003070 Fiji Downloads (imagej.net)
R – v4.2.2	R-project	SCR_000432 R: The R Project for Statistical Computing (r-project.org)
CutAdapt version 1.8.2	(Martin, 2011)[132]	Cutadapt — Cutadapt 4.7 documentation
ComBat-Seq	(Zhang et al., 2020)[133]	GitHub - zhangyuqing/ComBat-seq: Batch effect adjustment based on negative binomial regression for RNA sequencing count data
DESeq2 package	(Love et al., 2014)[134]	Bioconductor - DESeq2
pHeatmap package	(Kolde, 2019)[135]	CRAN - Package pheatmap (r-project.org)
clusterProfiler	(Yu et al., 2012)[136]	Bioconductor - clusterProfiler
ImageJ-based script for PLA analysis	(Heumuller et al.)[33]	N/A
Other		
Piston Gradient Fractionator	Biocomp	PISTON FRACTIONATION | Biocomp Instruments
Model EM-1 Econo UV detector	BioRad	7318160
Fraction collector	Gilson	170350
qPCR cycler CFX96	BioRad	1854095

REAGENT or RESOURCE	SOURCE	IDENTIFIER
NovaSeq6000 S1 100 cycle Flow Cell-v1.5	Illumina	NovaSeq 6000 System Specifications | Output, run time, and more (illumina.com)
iBlot2	Thermofisher	IB21001
Protein Simple	Kodak	Simple Western Systems - Automated Western Blots:: ProteinSimple